



Published in final edited form as:

J Comp Neurol. 2014 December 1; 522(17): 3861–3884. doi:10.1002/cne.23646.

DYNAMICS OF NASCENT AND ACTIVE ZONE ULTRASTRUCTURE AS SYNAPSES ENLARGE DURING LTP IN MATURE HIPPOCAMPUS

Maria Elizabeth Bell¹, Jennifer N. Bourne^{1,2}, Michael A. Chirillo^{1,3}, John M. Mendenhall¹, Masaaki Kuwajima¹, and Kristen M. Harris¹

¹Center for Learning and Memory, Department of Neuroscience, Institute for Neuroscience, University of Texas, Austin, TX 78712

³The University of Texas Medical School, Houston, TX 77030

Abstract

Nascent zones and active zones are adjacent synaptic regions that share a postsynaptic density, but nascent zones lack the presynaptic vesicles found at active zones. Here dendritic spine synapses were reconstructed through serial section electron microscopy (3DEM) and EM tomography to investigate nascent zone dynamics during long-term potentiation (LTP) in mature rat hippocampus. LTP was induced with theta-burst stimulation and comparisons were made to control stimulation in the same hippocampal slices at 5 minutes, 30 minutes, and 2 hours post-induction and to perfusion-fixed hippocampus *in vivo*. Nascent zones were present at the edges of ~35% of synapses in perfusion-fixed hippocampus and as many as ~50% of synapses in some hippocampal slice conditions. By 5 minutes, small dense core vesicles known to transport active zone proteins moved into more presynaptic boutons. By 30 minutes, nascent zone area decreased without significant change in synapse area, suggesting that presynaptic vesicles were recruited to pre-existing nascent zones. By 2 hours, both nascent and active zones were enlarged. Immunogold labeling revealed that glutamate receptors can be found in nascent zones; however, average distances from nascent zones to docked presynaptic vesicles ranged from 170±5 nm in perfusion-fixed hippocampus to 251±4 nm at enlarged synapses by 2 hours during LTP. Prior stochastic modeling suggests that falloff in glutamate concentration reduces the probability of glutamate receptor activation from 0.4 at the center of release to 0.1 just 200 nm away. Thus, conversion of nascent zones to functional active zones likely requires the recruitment of presynaptic vesicles during LTP.

Corresponding Author: Kristen M. Harris, PhD, University of Texas at Austin, Mail: 1 University Station C7000, Austin, TX 78712-0805, kmh2249@gmail.com, 512-232-3968.

²Current Address: Department of Physiology and Biophysics, University of Colorado, Anschutz Medical Campus, Aurora, CO 80045

Conflict of Interest Statement

The authors report no conflicts of interest

Role of Authors

MEB designed and performed all of the analyses with input from KMH. JNB performed the original LTP slice experiments and KMH provided the perfusion fixed tissue. MAC provided some of the DCV analyses. JMM and MK provided the EM Tomography, and MK performed the immunogold labeling. MEB and KMH prepared the figures and wrote the paper with input from all of the co-authors.

The authors declare no competing financial interests.

Keywords

Long-term potentiation; postsynaptic density; synaptic vesicles; synaptic plasticity; serial section electron microscopy; reconstruction; RRID:AB_2113447; RRID:AB_1769134; RRID:nif-0000-31686; RRID:nif-0000-23420

Introduction

We have identified an ultrastructurally distinct region at the edge of synapses in the intact mature hippocampus, the nascent zone, which was previously described as a vesicle-free transition zone (Spacek and Harris, 1998). Both nascent zones and active zones have a postsynaptic density (PSD), but unlike the active zone, the presynaptic side of a nascent zone lacks the small clear synaptic vesicles that are required for glutamate release. Synaptic edges are highly dynamic regions where AMPA-type glutamate receptors (AMPA-Rs), which mediate fast excitatory transmission, diffuse laterally until they are stabilized by activity (Choquet and Triller, 2013; MacGillavry et al., 2013). However, even if AMPA-Rs were present in a nascent zone, the absence of presynaptic vesicles could render the nascent zone functionally silent if glutamate released at an adjacent active zone did not reach sufficient concentration to activate those receptors (Christie and Jahr, 2006; Franks et al., 2003; MacGillavry et al., 2013; Nair et al., 2013; Raghavachari and Lisman, 2004). Thus, the recruitment of presynaptic vesicles to existing nascent zones could provide a mechanism for rapid enhancement of synaptic efficacy.

Enhancement of synaptic efficacy is investigated via long-term potentiation (LTP), which is widely thought to involve the same cellular mechanisms as those engaged during learning and memory (Bliss and Collingridge, 1993; Bourne and Harris, 2008; Yuste and Bonhoeffer, 2001). Following the induction of LTP, spine size, total PSD area, and the number of AMPA-Rs are known to increase (Bourne and Harris, 2011; Hering and Sheng, 2001; Lang et al., 2004; Luscher et al., 2000; Matsuzaki et al., 2001; Matsuzaki et al., 2004; Nagerl et al., 2004). Furthermore, LTP-related synapse enlargement can persist for hours to days (Fifkova and Anderson, 1981; Fifkova and Van Harreveld, 1977; Geinisman et al., 1993; Weeks et al., 2001) depending upon the functional status of the synapse during the induction of LTP (Macdougall and Fine, 2014). During LTP, receptors and other postsynaptic proteins are trafficked to the PSD (Luscher et al., 2000; Malinow and Malenka, 2002; Shi et al., 1999; Zhang and Lisman, 2012) and presynaptic neurotransmitter release is elevated (Bender et al., 2009; Bourne et al., 2013; Enoki et al., 2009; Ratnayaka et al., 2012). Presynaptic active zones must also be expanded as synapses enlarge during LTP. The substrate for this expansion could be provided by small dense core vesicles (DCVs), which are known to transport presynaptic scaffolding and other proteins needed for vesicle docking and release (Ahmari et al., 2000; Easley-Neal et al., 2013; Ehrlich et al., 2007; Oswald and Sigrist, 2009; Shapira et al., 2003; Sorra et al., 2006; Wu et al., 2013; Zhai et al., 2001). Furthermore, DCVs have been shown to contain N-cadherin (Zhai et al., 2001) and might also contain other cell adhesion molecules that anchor synapses and provide bidirectional signaling between synaptic partners (Benson and Huntley, 2010; Li and Sheng, 2003; McGeachie et al., 2011; Shipman and Nicoll, 2012). Insertion of DCVs at existing nascent

zones could initiate the recruitment of presynaptic vesicles necessary for the conversion of nascent zones to active zones. Whether DCVs are so mobilized during LTP has not previously been investigated.

Here we used reconstructions from 3DEM and EM tomography to investigate whether structural dynamics of nascent zones could serve to enhance synaptic efficacy following the induction of LTP in mature hippocampal area CA1. DCV frequency was measured along with nascent zone frequency and size to ascertain whether the timing of DCV mobilization was consistent with their hypothesized participation in the conversion of nascent zones to active zones. Immunogold labeling was performed to determine whether AMPARs were present in nascent zones. The number of presynaptic docked vesicles and their proximity to nascent zones were quantified to determine if glutamate diffusion from adjacent active zones could reliably activate nascent zone AMPARs or if, instead, the recruitment of presynaptic vesicles to nascent zones is required for functional activation.

Materials and Methods

Experimental Conditions

Hippocampal slices 400 μm thick were prepared from male Long-Evans rats aged 51–65 days old (weighing 219–361 g). The animals were anesthetized with halothane and decapitated, and slices were rapidly chopped from the middle third of the hippocampus. Slices were recovered in an interface chamber at 32°C for 3 hours prior to stimulation. A single recording electrode was positioned in the middle of *stratum radiatum* midway between two concentric bipolar stimulating electrodes (Figure 1, Fred Haer, Brunswick, ME, 100 μm outside diameter). The stimulating electrodes were separated by 600–800 μm to ensure site-specific LTP (Bourne and Harris, 2011; Ostroff et al., 2002; Sorra and Harris, 1998). Baseline and test pulse stimulations were alternated between the control and LTP electrode once every 2 minutes at a 30 second interval between electrodes. Theta-burst stimulation (TBS, 8 trains of 10 bursts at 5 Hz of 4 pulses at 100 Hz delivered 30 seconds apart) was delivered to one stimulating electrode at time 0 minutes (Figure 1). The site of TBS was alternated between the two stimulating electrodes across experiments. Extracellular field potentials were recorded and the initial slope of the field excitatory postsynaptic potential (fEPSP) was measured. Control stimulation was delivered to each electrode for approximately 30 minutes prior to TBS to ensure a stable baseline. Responses to test pulses were monitored at both control and LTP sites for 5 minutes ($n = 3$ slices from 3 animals), 30 minutes ($n = 3$ slices from 3 animals), or 2 hours ($n = 2$ slices from 2 animals) after delivery of the first TBS train (Figure 1, adapted from Bourne and Harris, 2011).

Processing and Imaging Through Serial Section Electron Microscopy

Slices with input-specific LTP were fixed at each time point, and time-series analyses were performed with 3DEM. Hippocampal slices were fixed immediately after recording by immersion in 6% glutaraldehyde and 2% paraformaldehyde in 0.1 M cacodylate buffer containing 2 mM CaCl_2 and 4 mM MgSO_4 during 10 seconds of microwave irradiation and were maintained at room temperature in the same fixative overnight (Bourne and Harris, 2011; Jensen and Harris, 1989). The slices were rinsed, embedded in agarose, trimmed to a

trapezoidal region of area CA1 that contained both of the stimulating electrodes, and vibrasliced at 70 μm (Leica VT 1000S, Leica, Nussloch, Germany). Vibra-slices showing a visible surface indentation and the two adjacent vibra-slices were processed for 3DEM through osmium tetroxide and potassium ferrocyanide, osmium tetroxide, uranyl acetate in ethanols, and propylene oxide, and embedded in LX-112 for 48 hours at 60°C according to our standard protocols (Bourne and Harris, 2011; Harris et al., 2006). Test thin sections that spanned the depth of the slice from air to net surface were taken and evaluated for high tissue quality at both the control and LTP sites. Of 24 experiments, 8 met strict ultrastructural criteria (Bourne and Harris, 2011) and were included in our analyses here. At least two hundred serial thin sections (45 nm) were cut in the center of the region with optimal preservation located 120–150 μm beneath the air surface and within 100 μm lateral to each stimulating electrode in the middle of *stratum radiatum*. These locations maximized the number of stimulated axons while ensuring input specificity and minimizing potential damage and direct depolarization of dendrites by the stimulating electrodes.

Perfusion-fixed hippocampus, which is the widely accepted gold standard for anatomical analyses, was used to establish baseline conditions (Lavenex et al., 2009; Miller, 1998; Roberts et al., 1990). Serial electron micrographs (EMs) were obtained from three adult male Long-Evans rats aged 68–77 days (weighing 310, 337, and 411 gm) from the middle of *stratum radiatum* in hippocampal area CA1 (Bourne et al., 2007; Harris et al., 1992; Harris and Stevens, 1989; Kirov and Harris, 1999; Mishchenko et al., 2010; Spacek and Harris, 1997). Briefly, intracardiac perfusion was performed under deep pentobarbital anesthesia, with fixative containing 2% paraformaldehyde, 2.5% or 6% glutaraldehyde, and 2 mM CaCl_2 in 0.1 M cacodylate buffer, pH 7.35, 37°C, and 4 psi backing pressure. After one hour, the hippocampus was removed. Perfusion-fixed samples of hippocampus were processed through osmium tetroxide and potassium ferrocyanide, followed by osmium tetroxide, and then dehydrated through graded ethanols with uranyl acetate, followed by propylene oxide, and embedded in LX-112 resin from which ultrathin serial sections were obtained (Harris et al., 2006, Reichert Ultracut, Leica, Deerfield, Illinois).

Serial sections were mounted on Pioloform-coated slot grids (Synaptek, Ted Pella) and counterstained with saturated ethanolic uranyl acetate and Reynolds lead citrate for 5 minutes each. Sections were imaged on a JEOL 1230 (or JEOL 1200) transmission electron microscope (Peabody, MA) with a calibration grid (Ted Pella Inc., Redding, CA) with a Gatan digital camera at a magnification of 5,000 \times and analyzed while blind to experimental condition. The serial section images were aligned and section thickness was computed using the cylindrical diameters method (Fiala and Harris, 2001a). Structures were traced and quantitative measurements and three-dimensional reconstructions were obtained using the RECONSTRUCT™ software (freely available for download at <http://synapses.clm.utexas.edu>, Fiala, 2005; Fiala and Harris, 2001b, RRID: nif-0000-23420).

EM Tomography

Area CA1 from perfusion-fixed hippocampus of a fourth adult male Long-Evans rat aged 164 days (weighing 474 gm) was processed and embedded into LX-112 resin as described above. Serial sections (~120 nm thickness) were cut and collected on slot grids coated with

polyetherimide (Goodfellow Corporation, Coraopolis, PA). Colloidal gold (10 nm diameter; Ted Pella) was applied to both sides of the sections to provide alignment fiducials. Single-axis tilt series ($\pm 60^\circ$ or 70° at 1° increment) of an axo-spinous synapse in the middle of *stratum radiatum* about $130\ \mu\text{m}$ from the CA1 pyramidal cell bodies were acquired over two consecutive sections with a Gatan UltraScan 4000 CCD camera mounted on a TEM at 120 kV (JEM-1400, JEOL) using SerialEM software (version 2.8.8, <http://bio3d.colorado.edu>). We used IMOD (version 4.5.7, <http://bio3d.colorado.edu>, RRID: nif-0000-31686) to generate tomograms with virtual sections $\sim 2\text{--}3\ \text{nm}$ thick. Some of these virtual sections were projected in the z-axis using FIJI (<http://fiji.sc/>) to simulate 50 nm thick sections. To compensate for the missing wedge effect, in which a spherical object would appear elongated in the z-axis of the tomogram, we used the largest diameter of small synaptic vesicles measured in x-y on single virtual sections as a reference (assuming spherical vesicles) to determine the number of virtual sections (50) to project in this simulation. RECONSTRUCTTM and FIJI were used to trace objects, compute measurements, and illustrate virtual sections from the tomograms. Closed traces on the tomographic virtual sections were obtained in RECONSTRUCTTM, exported as areas, and then opened as stacks in Fiji and rotated to be orthogonal to the virtual section planes.

Postembedding Immunogold Labeling of GluA1

Acute slices (thickness = $400\ \mu\text{m}$) were prepared from the left dorsal hippocampus of a male Long-Evans rat (age = P51; weight = 254 g) and recovered in ACSF in an interface chamber for 4 hours at 32°C before undergoing microwave-enhanced chemical fixation with a fixative solution containing 4% formaldehyde, 1% glutaraldehyde, 2 mM CaCl_2 , and 4 mM MgSO_4 in 0.1 M cacodylate buffer at $\text{pH} = 7.4$. The fixed slices were vibra-sliced into $200\ \mu\text{m}$ thickness, and tissue containing area CA1 was frozen at the rate of $>17,000^\circ\text{C/s}$ with a Leica EM PACT2 high-pressure freezer. Frozen tissue then underwent freeze-substitution in methanol containing 1.5% uranyl acetate for 60 hours at -90°C . After the temperature was raised to -50°C at 3°C/hr , the tissue was rinsed with methanol and infiltrated with HM20 resin (Electron Microscopy Sciences), which was then polymerized by UV light for 48 hours at -50°C . Serial ultrathin sections ($60\ \text{nm}$ thickness) were collected on gilded Synaptek grids coated with PEI film. The sections were incubated with 0.1% sodium borohydride and 50 mM glycine in filtered Tris-buffered saline (5 mM Tris and 0.3% NaCl, $\text{pH} = 7.6$) containing 0.01% Triton X-100 (TBS-T) and were rinsed in filtered TBS-T five times over 30 minutes. The sections were then blocked with human serum albumin (HSA; 2% in filtered TBS-T) for 10 minutes before incubation in affinity-purified polyclonal rabbit anti-GluA1 IgG (Abcam, Cat# ab31232, RRID: AB_2113447; Lot 789940) and diluted to $24\ \mu\text{g/ml}$ in filtered TBS-T with 2% HSA for 2 hours at room temperature. After quick rinses in filtered TBS-T, the sections were blocked again with 2% HSA for 10 minutes and incubated with goat anti-rabbit IgG conjugated with 15 nm colloidal gold (BBInternational, Cat# EM GAR15/1, RRID: AB_1769134; Lot 16140; 1:100 in filtered TBS-T with 2% HSA and 0.5% polyethylene glycol) for 2 hours at room temperature. The sections were then rinsed three times in filtered TBS-T and five times in filtered purified water before being stained with uranyl acetate and lead citrate for EM observation.

The anti-GluA1 IgG was raised against synthetic peptide containing amino acids 850 to the C-terminus of human GluA1 protein. This antibody detected a single band at ~100 kDa from mouse hippocampus lysate in a Western blot analysis and strongly labeled Purkinje cell dendrites in formaldehyde-fixed paraffin-embedded rat cerebellum sections, suggesting its high specificity (according to the manufacturer's datasheet available at <http://www.abcam.com/glutamate-receptor-1-ampa-subtype-antibody-ab31232.html>). It was also used for immunofluorescence detection of synaptic GluA1 in formaldehyde-fixed cryostat sections from the mouse hippocampus using stochastic optical reconstruction microscopy (Dani et al., 2010). We performed a negative control on our HM20-embedded tissue by omitting the primary antibody, which resulted in a low level of background staining due to the non-specific binding of the gold-conjugated secondary antibody, which was present only in mitochondria and in no other parts of the tissue, including synapses. A PSD was deemed immuno-positive when it was labeled through at least three serial sections.

Sample Dendrites and Presynaptic Vesicles

In both perfusion-fixed and slice tissue, cross-sectioned dendritic segments were selected for analysis. In order to ensure that differences in dendrite caliber did not have an impact on spine density, the sample dendrites from all conditions ranged from 0.4–0.8 μm in diameter and had 7–23 microtubules (Bourne and Harris, 2011; Harris et al., 2007). Representative presynaptic vesicles were selected for measurement in Figure 2 using the same strategy as described in Sorra et al. (2006). Namely, small synaptic vesicles that were nearest neighbors to a dense core vesicle in a presynaptic bouton were measured from each series by tracing the outer circumference (C) and calculating the diameter ($D = C/\pi$), assuming spherical vesicles.

Statistical Analyses

Statistical analyses were done in the STATISTICA software package (StatSoft, Tulsa, OK). For most of the reported results, we used the hierarchical nested ANOVA (hnANOVA), which allowed us to determine that none of the results were driven by a particular dendrite or experiment, and reduced the degrees of freedom of analyzed synapses by one for each dendrite and by one for each experiment and condition. Natural log-transforms of the surface areas of PSDs, active zones, and nascent zones as well as docked vesicle number and distance to nascent zones were applied to normalize these skewed distributions before computing hnANOVAs.

Since control stimulation resulted in significant differences across time *in vitro*, all of the LTP-related comparisons were made using the hnANOVA within a particular time point, with dendrite nested in condition and experiment, and experiment nested in condition. These time-matched comparisons were appropriate since control and TBS stimulation were delivered within the same slice for each experiment.

When comparing area measurements in slices to perfusion-fixed data, hnANOVAs were performed across 2 groups (perfusion-fixed and 5 or 30 minute data collapsed across condition), 3 groups (perfusion-fixed, 2 hour control, and 2 hour LTP conditions), or 4 groups (perfusion-fixed and control conditions from 3 time points), with dendrite nested in

group and experiment, and experiment nested in group. Similarly, when comparing area measurements across control slices, hnANOVAs were performed across 3 groups (3 time points), with dendrite nested in group and experiment, and experiment nested in group. For 3 and 4 group comparisons, the Tukey's HSD post-hoc test was then applied to determine differences between each of the groups.

ANCOVAs were used to determine the strength and effects of LTP on the relationships between PSD and nascent zone areas and docked vesicle numbers and active zone areas. Log-transformations were not applied when computing ANCOVAs.

The outcomes of statistical tests are reported in the results, figure legends, and tables where appropriate. For each finding the type of test used, the statistical value achieved, n values, degrees of freedom, and p values are reported with significance set at $p < 0.05$. Unless otherwise indicated, data are reported or plotted as the mean \pm SEM from the actual measurements (not log-transforms). Active zone is abbreviated as AZ and nascent zone is abbreviated as NZ in the figures and legends but spelled out elsewhere for ease of reading.

Results

Identification of Nascent Zones

Criteria for distinguishing nascent zones from active zones were first established in perfusion-fixed hippocampus and then applied to the control and LTP sites in the hippocampal slices. A nascent zone was qualitatively identified as having a PSD that was similar in ultrastructure to the PSD of the adjacent active zone but lacking the docked and nondocked presynaptic vesicles that congregated at the active zone (Figure 2A–E). A portion of the active zone might have been mistaken for a nascent zone if a docked vesicle had been released immediately prior to fixation; however, docked vesicles typically were not found in isolation without neighboring nondocked vesicles. Hence, to avoid potential misidentification of nascent zones, we set a conservative criterion for the minimum nascent zone length on each section as the width of two presynaptic vesicles and required that no vesicles were located within two vesicle diameters perpendicular to the presynaptic membrane along a nascent zone. Representative cross-sectioned vesicles were selected to quantify these criteria (see Methods). No significant differences in vesicle diameters were found across series for any of the conditions (Figure 2F), and the criterion vesicle diameter was set as the mean of perfusion-fixed hippocampus (47 ± 1 nm, comparable to previous findings from Sorra et al., 2006). Thus, the minimum nascent zone was 94 nm long on a single section with an area of $0.004 \mu\text{m}^2$ across all conditions. Although some nascent zones might have been missed if sectioned *en face*, only 3 synapses (0.25%) were composed entirely of nascent zone area (0.0068 , 0.0077 , and $0.013 \mu\text{m}^2$). Thus, it is unlikely that this approach underestimated active zones, and it provided a conservative, unbiased estimate of nascent zone areas. 3DEM revealed that some synapses had more than one nascent zone (Figure 2G, H); therefore, the summed nascent zone area per synapse was usually compared across conditions, except where analysis of individual nascent zone areas was applicable and is explicitly stated below.

An additional approach using higher-resolution EM tomography served to estimate the accuracy of identifying and measuring nascent zones through the ~50 nm serial sections used in this study. Tomograms were generated from two serial sections (each ~120 nm thick) through part of a large synapse with a nascent zone in perfusion-fixed hippocampus, (Figure 3). Virtual sections were simulated at ~2–3 nm (210 sections) or ~50 nm (4 sections) from the same tomograms for comparison. When viewed through the ~2–3 nm virtual sections, docked vesicles with pores (Figure 3A–D) or without pores (Figure 3E, F) in the presynaptic membrane were readily identified at the active zone. No vesicles were located within 94 nm perpendicular to the presynaptic membrane of the nascent zone in any of the ~2–3 or ~50 nm virtual sections (Figure 3G). The measured dimensions of the nascent zone were the same ($0.017 \mu\text{m}^2$) within measurement error in the ~2–3 nm (aqua region) and the ~50 nm virtual sections (region bounded by dashed white outline, Figure 3G), although the boundaries were more precise in the thinner virtual sections. Based on these comparisons, we concluded that 3DEM using ~50 nm section thickness provides reliable identification and measurement of nascent zones.

When synapses were imaged in cross-section, as in Figures 2 and 3, the distinction between nascent and active zones was obvious. However, if a synapse was sectioned obliquely, then the PSD could have obscured presynaptic vesicles within the section (Figure 4A, B). Therefore, only cross-sectioned synapses were used in these analyses (Figure 4C). The average PSD area of the cross-sectioned subset of synapses was significantly less than that of the overall population because larger synapses are more often curved and obliquely sectioned; however, the number of cross-sectioned synapses still represented a major fraction of the overall sample (Figure 4D).

Since cross-sectioned synapses were on average smaller, we determined whether the sample of cross-sectioned synapses (Table 1) produced the same results as previously reported for the set of all synapses (Bourne and Harris, 2011). The average cross-sectioned PSD area was substantially enlarged by 2 hours after induction of LTP relative to control stimulation, but not at 5 or 30 minutes, which was consistent with the overall population of synapses (Figure 4E). Thus, the cross-sectioned population of synapses provided a representative sample for analysis of nascent zones.

Nascent Zone Frequency and Changes with Constitutive Synaptogenesis

Some synapses had no nascent zones (Figure 5Ai–iv, B), but at synapses where they were present, nascent zones were located primarily at the outer edges of active zones (Figure 5C, D). A greater percentage of synapses in the 30 minute and 2 hour conditions had nascent zones than in the 5 minute and perfusion-fixed conditions, but there was no effect of LTP on this percentage at any time point (Figure 5E). This increase could have resulted from differences in the total amount of stimulation received over time under the control or LTP conditions, or instead from passive differences in the degree of recovery due to the total time spent *in vitro*.

Thus the question arose as to whether this proliferation of nascent zones was related to constitutive synaptogenesis in slices. We knew from our prior work that slices must be recovered *in vitro* for at least 3 hours, as was done in these experiments, to achieve near-

perfusion quality tissue (Bourne and Harris, 2012b; Bourne et al., 2007; Fiala et al., 2003). When we compared cross-sectioned PSD area measurements in slices and perfusion-fixed hippocampus, we detected significant differences (Figure 6). There was no LTP effect at 5 or 30 minutes, but when the data were collapsed across conditions, the mean PSD area was significantly increased relative to perfusion-fixed hippocampus at both times (Figure 6A). Interestingly, PSD area returned to perfusion-fixed levels by 2 hours in the control condition (Figure 6A). In the 2 hour LTP condition, PSD area was significantly increased relative both to perfusion-fixed hippocampus and the time-matched control (Figure 6A). Comparison across control conditions revealed that this effect was not due to a change in the size of synapses on small (head diameter $<0.45 \mu\text{m}$) or large dendritic spines (head diameter $0.45 \mu\text{m}$, Figure 6B) but instead resulted from the addition of small dendritic spines in the 2 hour control condition (Figure 6C, re-plotted from Bourne and Harris, 2011). Since the physiological response to control stimulation did not change over time (Figure 1), it seems unlikely that the additional small spine synapses were functional. These findings show that synapse number and average PSD area returned to perfusion-fixed levels by 2 hours in slices that received control stimulation only. In contrast, TBS resulted in PSD enlargement by 2 hours after the induction of LTP. As noted in Bourne and Harris, 2011, by 2 hours after the induction of LTP, the return of dendritic spines to *in vivo* levels was either prevented or spines were eliminated following TBS stimulation.

One might argue that the changes in synapse number with time and test pulse delivery precluded the analysis of potentiation-related effects, especially since spine density decreased relative to perfusion-fixed hippocampus in the 5 and 30 minute control conditions. However, because all LTP-related comparisons were made within the same slices, and therefore after the same amount of time *in vitro*, it was possible to distinguish the effects of TBS from those due to the delivery of test pulse stimulation. Therefore, results from all three time points are reported below.

Influence of Nascent Zones on Active Zone Dynamics

Next, we determined whether the absence or presence of a nascent zone would affect active zone size (Figure 7). At synapses without nascent zones, active zone areas were not significantly different from perfusion-fixed hippocampus at any time point or condition, with the exception of the 2 hour LTP condition, in which active zones were significantly enlarged relative to both time-matched control and perfusion-fixed hippocampus (Figure 7A). In contrast, when combined across condition, the active zones of synapses with nascent zones were significantly larger at both 5 minutes and 30 minutes relative to perfusion-fixed hippocampus (Figure 7B). Furthermore, the active zones were also significantly enlarged at 2 hours during LTP relative to both time-matched control and perfusion-fixed hippocampus (Figure 7B). These results suggest that, relative to perfusion-fixed hippocampus, active zones were larger and more dynamic at synapses with nascent zones in hippocampal slices early during constitutive synaptogenesis and at 2 hours following induction of LTP.

Effects of LTP on Nascent Zone Area

Under all conditions and times, the summed nascent zone area per synapse was positively and significantly correlated with PSD area (Figure 8A–C). There was no significant

difference in summed nascent zone area per synapse relative to perfusion-fixed hippocampus under control conditions at any time point. At 5 minutes after the induction of LTP, the number and size of nascent zones were unchanged relative to time-matched control conditions across synapses of all sizes (Table 1, Figure 8A). By 30 minutes, there were fewer nascent zones per synapse in the LTP condition than in the time-matched control (Table 1), resulting in a smaller summed nascent zone area per synapse (Figure 8B). By 2 hours during LTP, individual nascent zone area increased relative to time matched control (Table 1), resulting in a significant increase in the summed nascent zone area per synapse (Figure 8C). These findings suggest that nascent zones were converted to active zones via recruitment of presynaptic vesicles by 30 minutes after LTP induction, while average PSD area remained unaltered, and that NZs were restored and enlarged by 2 hours during LTP.

Potential Involvement of Nascent Zone Conversion in Active Zone Enlargement

To test the plausibility of the nascent zone conversion and growth hypothesis, we sought to compute the number of nascent zones that would need to be converted to account for active zone enlargement at 2 hours during LTP (Figure 9). Synapse size scales with spine size (Harris and Stevens, 1989; Hering and Sheng, 2001), and spines can enlarge rapidly during LTP, even before PSD areas grow (Bourne and Harris, 2011; Matsuzaki et al., 2001; Matsuzaki et al., 2004). Synapses of different sizes might require different amounts of nascent zone conversion to account for their active zone enlargement; hence, we set the median spine head diameter in the 2 hour control condition ($0.36\ \mu\text{m}$) as the criterion to split spines into small and large categories. For small spines, the active zone enlargement would require conversion of 1.2 times the mean, but only 0.46 times the largest summed nascent zone area (Figure 9A). For large spines, the active zone enlargement would require conversion of 3.2 times the mean, but only 0.76 times the largest summed nascent zone area (Figure 9B). Thus, summed nascent zone areas found at control synapses were sufficient to account for active zone growth by nascent zone conversion on both small and large spines by 2 hours during LTP.

Role for Small Dense Core Vesicles in Nascent Zone Conversion

Presynaptic active zone proteins are transported in the membranes of small ($\sim 80\ \text{nm}$) dense core vesicles (DCVs, Shapira et al., 2003; Zhai et al., 2001). DCVs travel between axonal boutons in transport packets (Ahmari et al., 2000; Bourne et al., 2013; Dresbach et al., 2006; Maas et al., 2012; Sorra et al., 2006; Wu et al., 2013; Ziv and Garner, 2001), allowing for their redistribution from other locations to boutons that might require the formation or growth of presynaptic active zones. Our previous work showed that DCVs were present in 26% of presynaptic axonal boutons in perfusion-fixed mature hippocampal area CA1 and decreased to 17% during constitutive synaptogenesis during recovery in hippocampal slices (Sorra et al., 2006). Here, presynaptic boutons were viewed through serial sections until they became clearly tapered on each end. Individual boutons contained 0–8 DCVs (Fig. 10A, Table 2). Given the transience of the process, capturing DCVs in the act of releasing their contents was a rare event (Fig 10B). We hypothesized that DCVs provide rapid delivery of presynaptic active zone components to nascent zones as part of the conversion process as active zones enlarge during LTP in the mature hippocampus (Figure 10C). Consistent with this hypothesis, the percentage of presynaptic boutons containing DCVs increased

significantly at 5 minutes and returned to time-matched control levels by 30 minutes after the induction of LTP (Figure 10D).

The low number of DCVs per bouton suggests that rarely would more than one be released at the same location. Hence, in order for our hypothesis to be correct, the surface area of a single DCV would need to convert an entire nascent zone to active zone. DCVs were large enough to span more than one section. DCV circumferences (C) were measured on the section with a clear bounding membrane, their diameters were calculated ($D = C/\pi$), and their surface areas were computed assuming that they were spherical ($SA = \pi D^2$). The mean DCV diameter in slices was 80.0 ± 0.0004 nm, which did not differ significantly across conditions or time point and was comparable to prior findings (Sorra et al., 2006). The surface area of a single DCV (Figure 10E) was greater than most individual nascent zone areas (Table 1), thus insertion of one presynaptic DCV would be more than sufficient to convert most nascent zones to active zones in both LTP and time-matched control conditions at 30 minutes (Figure 10F) and 2 hours during LTP (Figure 10G).

Together these findings suggest that DCVs could migrate rapidly from inter-bouton regions to presynaptic boutons, where their release between 5 and 30 minutes would usually be sufficient to convert existing nascent zones to active zones. Given that DCV surface areas are frequently larger than individual nascent zones, the extra presynaptic material they provide might also serve to initiate addition and growth of nascent zones, as was also observed at 2 hours during LTP (see Figure 8C and Table 1).

Implications of Altered Docked Vesicle Distribution at Enlarged Active Zones

Prior work has shown that the number of presynaptic vesicles correlates nearly perfectly with the total PSD area per synapse (Harris and Sultan, 1995; Lisman and Harris, 1993; Schikorski and Stevens, 1997). Recently we found that by 30 minutes following TBS the number of vesicles docked at synapses decreased, and that by 2 hours vesicle pools were also smaller, especially in boutons with coated pits or vesicles demonstrating recent recycling activity (Bourne et al., 2013).

Here we determined the density and distribution of docked vesicles as active zones enlarged during LTP (Figure 11). At 5 minutes after induction of LTP, there was no change in the number or density of docked vesicles at active zones (Table 2, Figure 11A). By 30 minutes, there was a significant decrease in the number and density of docked vesicles per active zone (Table 2, Figure 11B). This decrease in docked vesicles suggests an increase in presynaptic release, which is consistent with the observation that additional vesicles were recruited to within 94 nm of the presynaptic membrane at 30 minutes following LTP induction, resulting in the reduction of summed nascent zone area (see Figure 8B). By 2 hours during LTP, the total number of docked vesicles per active zone returned to time-matched control levels, but the contemporaneous increase in active zone area resulted in a decrease in the density of docked vesicles at active zones on synapses of all sizes (Tables 1 and 2 and Figure 11C, D). The correlation between docked vesicles and active zone area was highly significant across all times and conditions, suggesting that an elevated release of docked vesicles had occurred uniformly across pre-existing and recently converted active zones.

Functional Status of Nascent Zones

Glutamatergic synapses are functionally silent if they lack AMPARs, which mediate fast excitatory transmission and accumulate in synapses during LTP (Bredt and Nicoll, 2003; Collingridge et al., 2004; Isaac et al., 1995; Kerchner and Nicoll, 2008; Kim et al., 2003; Liao et al., 1995; Malinow and Malenka, 2002; Sheng and Kim, 2002; Shepherd and Huganir, 2007). Their functional status also depends on whether AMPARs are near enough to docking sites to detect glutamate released from presynaptic vesicles (Christie and Jahr, 2006; Raghavachari and Lisman, 2004; Traynelis et al., 2010). Stochastic modeling of synapses with a random distribution of glutamate receptors using MCell (<http://mcell.org>) showed that the probability of an AMPA-type channel opening upon release of presynaptic glutamate falls off exponentially from 0.4 at the center of a release site to just 0.1 at a distance 200 nm away (Franks et al., 2003; Kinney et al., 2013).

We hypothesized that recruitment of presynaptic vesicles to nascent zones was necessary to switch them from a functionally silent to an activatable state. As predicted from visualization of AMPARs in cultured neurons (Nair et al., 2013), we have determined with immunogold labeling (Figure 12A–D) that AMPARs can be found in nascent zones of mature synapses (Figure 12B). To test the vesicle recruitment hypothesis, we computed the minimum distance in 3D from every vesicle docked at an active zone to the nearest edge of nascent zone(s) on the same synapse using RECONSTRUCT™ (Figure 12E). The distribution of these distances ranged from 14 nm (vesicle docked immediately adjacent to the nascent zone) to more than 1000 nm (Figure 12F). On average, the minimum distances were 170 ± 5 nm at perfusion-fixed synapses, 214 ± 6 nm in the 2 hour control condition, and increased to 251 ± 4 nm in the 2 hour LTP condition due to synapse enlargement (Figure 12G). These measurements suggest that an AMPAR in a nascent zone would have a much lower probability of response than AMPARs anchored beneath docking sites in the active zone (Franks et al., 2003). Thus, recruitment of presynaptic vesicles to nascent zones during LTP should indeed be needed to achieve the enhanced synaptic efficacy.

Discussion

These results demonstrate that nascent zones are dynamic substrates for LTP-induced synapse enlargement in mature hippocampus. Based on these findings, we propose a model of structural synaptic plasticity in which synapse enlargement occurs via nascent to active zone conversion following induction of LTP (Figure 13). By 5 minutes after TBS, small DCVs moved into more presynaptic boutons. The return of their frequency to control levels by 30 minutes suggests that DCVs could have been released at existing nascent zones, initiating nascent to active zone conversion via the recruitment of small presynaptic vesicles. As the surface area of a single DCV is greater than that of most individual nascent zones, proteins on DCV surface membranes and in their cores could provide a substrate for the additional growth of nascent and active zones during LTP. Mechanisms of postsynaptic growth could involve synthesis of new proteins or redistribution of existing synaptic resources, such as those from eliminated small spine synapses (Bourne and Harris, 2011; Bourne and Harris, 2012a; Harvey et al., 2008). In light of prior modeling studies (Franks et al., 2002; Franks et al., 2003), the measured distances from presynaptic vesicles docked in

active zones to adjacent nascent zones suggest that many nascent zones are functionally silent. Therefore the recruitment and release of presynaptic vesicles at existing nascent zones is crucial to provide sufficient glutamate to stabilize mobile AMPARs and convert silent nascent zones to responsive active zones (Choquet and Triller, 2013; Lisman and Raghavachari, 2006).

Because living neurons cannot be visualized in the electron microscope, time-series 3DEM was required to reveal ultrastructural changes in nascent zones and active zones that were present as synapses enlarged during LTP in the mature hippocampus. Due to their small size, distinguishing nascent zones from active zones with light microscopy will require new knowledge of which molecules, if any, are specific to each zone and when they might move freely between the zones (Deane et al., 2013; MacGillavry et al., 2013; Nair et al., 2013). Such studies could become possible given advances in super-resolution fluorescence microscopy, which have revealed dynamic changes in spine morphology at up to 43 nm resolution *in vivo* (Willig et al., 2014). Furthermore, a better understanding of the potential for activation of nascent zone receptors via glutamate diffusion will require the z-axis resolution currently only achieved with EM tomography due to the non-uniformity of the dimensions and composition of the synaptic cleft (Chen et al., 2008; Harlow et al., 2001). The evidence presented here provides motivation for the further refinement of both light and electron microscopy methods to investigate nascent zone dynamics as a general mechanism for synaptic plasticity in living mature circuits.

Postsynaptically silent synapses are commonly found in the developing nervous system, and they undergo un-silencing by the insertion or functional modification of AMPARs during LTP (Durand et al., 1996; Edwards, 1991; Groc et al., 2006; Hanse et al., 2009; Isaac et al., 1995; Liao et al., 1995; Macdougall and Fine, 2014; Petralia et al., 1999). Other junctions, including nascent synapses and surface specializations, have a distinct PSD but no presynaptic vesicles and are present frequently in the developing but not the mature hippocampus (Ahmari and Smith, 2002; Fiala et al., 1998; Vaughn, 1989). Small DCVs, alone or in combination with small presynaptic vesicles, are transported to and inserted at nascent synapses, which are soon thereafter converted to functional synapses (Ahmari et al., 2000; Buchanan et al., 1989; Sabo et al., 2006; Zhai et al., 2001; Ziv and Garner, 2004). Thus, the processes by which new synapses are formed during development are consistent with our model of the conversion of nascent zones to active zones at enlarging synapses in the mature system.

In support of our hypothesis that DCVs contribute to nascent zone conversion, DCVs are known to transport a variety of active zone proteins as well as cell adhesion molecules (CAMs, Zhai et al., 2001). CAMs are proteins involved in bidirectional signaling and coordinated recruitment of pre- and postsynaptic proteins and receptors (Akins and Biederer, 2006; Benson and Huntley, 2010; Benson et al., 2000; Li and Sheng, 2003; Scheiffele, 2003; Sytnyk et al., 2002; Waites et al., 2005; Ziv and Garner, 2004). DCVs contain cadherins (Zhai et al., 2001), which cluster at the edges of synapses (Elste and Benson, 2006; Fannon and Colman, 1996; Uchida et al., 1996), regulate AMPAR trafficking (Nuriya and Huganir, 2006; Saglietti et al., 2007; Zhai et al., 2001), and are required to stabilize enhanced synaptic efficacy during LTP (Bozdagi et al., 2000; Bozdagi et al., 2010; Mendez et al., 2010; Tang

et al., 1998). DCVs could transport other presynaptic CAMs that might also participate in nascent zone conversion. For example, neuroligin-1 (NLG-1) or postsynaptic leucine-rich repeat transmembrane protein 2 (LRRTM2). This extracellular binding modulates presynaptic vesicle release probability and promotes synapse initiation and stabilization via transsynaptic signaling in cooperation with N-cadherin (Dean et al., 2003; deWit J. et al., 2009; Futai et al., 2007; Graf et al., 2004; Heine et al., 2008; Ichtchenko et al., 1995; Linhoff et al., 2009; Scheiffele et al., 2000; Soler-Llavina et al., 2013; Song et al., 1999; Stan et al., 2010; Sudhof, 2008; Wittenmayer et al., 2009). In addition, the *Nrx-1* β /*NLG-1* complex binds with PSD-95, Stargazin, and other proteins that reduce AMPAR diffusion (Barrow et al., 2009; Giannone et al., 2013; Irie et al., 1997; Mondin et al., 2011; Sudhof, 2008). Presynaptic ephrin-B is another strong candidate for DCV transport and nascent zone conversion because its extracellular binding to postsynaptic EphB receptors has been implicated in the modulation of the synaptic vesicle cycle and recruitment of glutamate receptors to synapses during maturation and plasticity (Henkemeyer et al., 2003; Kayser et al., 2006; Klein, 2009; Lai and Ip, 2009; Lim et al., 2008; Murata and Constantine-Paton, 2013; Nolt et al., 2011). Which DCV-transported proteins are specifically engaged in nascent zone conversion and growth at mature synapses remains to be determined.

From the postsynaptic perspective, nascent zones could host a variety of proteins that could trap AMPARs upon appropriate signaling (Lisman and Raghavachari, 2006; Opazo and Choquet, 2011; Opazo et al., 2010; Zhang and Lisman, 2012). Recent work in cultured neurons suggests that the distribution of such synaptic proteins is non-uniform and highly dynamic (MacGillavry et al., 2013). AMPARs are inserted at extrasynaptic regions and then diffuse along the spine membrane to the synapse during LTP (Ashby et al., 2006; Bassani et al., 2013; Makino and Malinow, 2009; Shi et al., 1999). Single-particle tracking studies in cultured neurons show that AMPARs are highly mobile at inactive synapses, whereas local synaptic activity (Derkach et al., 2007; Ehlers et al., 2007; Nair et al., 2013), involving PSD-95 and Stargazin phosphorylated by CAMKII (Opazo et al., 2010), causes them to stabilize. Thus, the stabilization of AMPARs in existing active zones or converted nascent zones could account for a rapid, yet stable, level of potentiation of the fEPSP observed across 5 minutes to 2 hours following the induction of LTP.

We show that changes in synapse structure occur without concurrent changes in the slope of the fEPSP. At the control stimulation sites, the number of small dendritic spines was significantly increased by 2 hours, relative to 5 minutes, despite no change in the magnitude of the fEPSP. This result suggests that the additional small spine synapses were silent. By 2 hours after the induction of LTP, small spines were either eliminated or their formation was prevented (Bourne and Harris, 2011). Both nascent and active zones at the remaining synapses were added or enlarged. Since the level of potentiation remained stable and nascent zones are likely to be silent, these results suggest that the enlarged active zones must also be partially silent. Hippocampal CA3 \rightarrow CA1 synapses have low probabilities of vesicular release and glutamate receptor activation (Allen and Stevens, 1994; Bekkers and Stevens, 1995; Franks et al., 2002; Franks et al., 2003; Liu et al., 1999; McAllister and Stevens, 2000). We considered how changes in the density of presynaptic docked vesicles, as an estimate of the density of release sites, might affect the postsynaptic response. We found

that the docked vesicle density decreased across the enlarged active zone areas at 2 hours during LTP relative to control stimulation in the same slices. Therefore, as the postsynaptic area enlarged, presynaptic vesicle docking sites become more sparsely distributed. Consequently, the number of activated receptors might remain constant due to drops in glutamate concentrations in the synaptic cleft as active zones enlarge, resulting in a stably potentiated response across time.

Since the enlargement of nascent and active zones at 2 hours following induction of LTP does not appear to have enhanced the potentiation at that time, then perhaps it prepares synapses for subsequent augmentation of LTP. Recent findings show that delivery of a single episode of TBS can saturate LTP, such that subsequent episodes delivered less than 30 minutes later produce no additional potentiation (Lynch et al., 2013). However, if the delay between episodes is 1 hour or more, additional episodes of TBS can augment LTP (Cao and Harris, 2012; Kramar et al., 2012). These spaced episodes of LTP induction have been proposed as a model for understanding the mechanisms of spaced learning (Lynch and Gall, 2013; Lynch et al., 2013). Spaced learning produces longer memories than massed learning, and the efficacy of memory is dependent on the interval between repetitions (Ebbinghaus, 1885; Ruger and Bussenius, 1913). The delay required to allow augmentation of LTP is consistent with the ~30 minutes to 2 hours following LTP induction during which both nascent and active zones enlarged. Therefore nascent and active zone growth could be the substrate for the augmentation of LTP that occurs with sufficiently spaced TBS episodes and an underlying mechanism of spaced learning.

In summary, these findings suggest that nascent zone conversion could provide a rapid mechanism for synapse growth in the mature hippocampus. Conversion of nascent zones to active zones begins prior to PSD enlargement and entails the recruitment of presynaptic vesicles to existing nascent zones. This process appears to be facilitated by the insertion of presynaptic active zone proteins delivered through the release of small DCVs shortly after induction of LTP. Nascent zone conversion likely corresponds to the un-silencing of functionally inactive regions at mature synapses and proceeds in a manner similar to synapse formation during development. Whether the addition of nascent and active zone area provides a basis for further enhancement of synaptic efficacy presents an intriguing question for future investigation into the structural basis of memory.

Acknowledgments

Support

This work was supported by NIH Grants NS21184, MH095980, and NS074644 to KMH, NS71442 to JNB, and the Texas Emerging Technologies Fund.

We thank Dr. Guan Cao for providing tissue for the immunogold labeling and Dr. Deborah Watson, Dr. Randy Chitwood, and members of the Harris lab for insightful comments.

References Cited

Ahmari SE, Buchanan J, Smith SJ. Assembly of presynaptic active zones from cytoplasmic transport packets. *Nat Neurosci.* 2000; 3(5):445–51. [PubMed: 10769383]

- Ahmari SE, Smith SJ. Knowing a nascent synapse when you see it. *Neuron*. 2002; 34(3):333–6. [PubMed: 11988164]
- Akins MR, Biederer T. Cell-cell interactions in synaptogenesis. *Curr Opin Neurobiol*. 2006; 16(1):83–9. [PubMed: 16427268]
- Allen C, Stevens CF. An evaluation of causes for unreliability of synaptic transmission. *Proc Natl Acad Sci U S A*. 1994; 91(22):10380–3. [PubMed: 7937958]
- Ashby MC, Maier SR, Nishimune A, Henley JM. Lateral diffusion drives constitutive exchange of AMPA receptors at dendritic spines and is regulated by spine morphology. *J Neurosci*. 2006; 26:7046–55. [PubMed: 16807334]
- Barrow SL, Constable JR, Clark E, El-Sabeawy F, McAllister AK, Washbourne P. Neuroigin1: a cell adhesion molecule that recruits PSD-95 and NMDA receptors by distinct mechanisms during synaptogenesis. *Neural Dev*. 2009; 4:17. [PubMed: 19450252]
- Bassani S, Folci A, Zapata J, Passafaro M. 2013AMPA trafficking in synapse maturation and plasticity. *Cell Mol Life Sci*.
- Bekkers JM, Stevens CF. Quantal analysis of EPSCs recorded from small numbers of synapses in hippocampal cultures. *J Neurophysiol*. 1995; 73(3):1145–56. [PubMed: 7608761]
- Bender VA, Pugh JR, Jahr CE. Presynaptically expressed long-term potentiation increases multivesicular release at parallel fiber synapses 3. *J Neurosci*. 2009; 29(35):10974–8. [PubMed: 19726655]
- Benson DL, Huntley GW. Building and remodeling synapses. *Hippocampus*. 2010
- Benson DL, Schnapp LM, Shapiro L, Huntley GW. Making memories stick: cell-adhesion molecules in synaptic plasticity. *Trends Cell Biol*. 2000; 10(11):473–82. [PubMed: 11050419]
- Bliss TV, Collingridge GL. A synaptic model of memory: long-term potentiation in the hippocampus. *Nature*. 1993; 361(6407):31–9. [PubMed: 8421494]
- Bourne JN, Chirillo MA, Harris KM. Presynaptic ultrastructural plasticity along CA3→CA1 axons during LTP in mature hippocampus. *J Comp Neurol*. 2013 Jun 20.10.1002/cne23384
- Bourne JN, Harris KM. Balancing structure and function at hippocampal dendritic spines. *Annu Rev Neurosci*. 2008; 31:47–67. [PubMed: 18284372]
- Bourne JN, Harris KM. Coordination of size and number of excitatory and inhibitory synapses results in a balanced structural plasticity along mature hippocampal CA1 dendrites during LTP. *Hippocampus*. 2011; 21(4):354–73. [PubMed: 20101601]
- Bourne JN, Harris KM. Changes in the Complexity and volume of smooth endoplasmic reticulum are coupled with synaptic enlargement along mature hippocampal dendrites during LTP. *Soc Neuroscience Abs # 145.05*. 2012a
- Bourne JN, Harris KM. Nanoscale analysis of structural synaptic plasticity. *Curr Opin Neurobiol*. 2012b; 22(3):372–82. [PubMed: 22088391]
- Bourne JN, Kirov SA, Sorra KE, Harris KM. Warmer preparation of hippocampal slices prevents synapse proliferation that might obscure LTP-related structural plasticity. *Neuropharmacology*. 2007; 52(1):55–9. [PubMed: 16895730]
- Bozdagi O, Shan W, Tanaka H, Benson DL, Huntley GW. Increasing numbers of synaptic puncta during late-phase LTP: N-cadherin is synthesized, recruited to synaptic sites, and required for potentiation. *Neuron*. 2000; 28(1):245–59. [PubMed: 11086998]
- Bozdagi O, Wang XB, Nikitczuk JS, Anderson TR, Bloss EB, Radice GL, Zhou Q, Benson DL, Huntley GW. Persistence of coordinated long-term potentiation and dendritic spine enlargement at mature hippocampal CA1 synapses requires N-cadherin. *J Neurosci*. 2010; 30(30):9984–9. [PubMed: 20668183]
- Bredt DS, Nicoll RA. AMPA receptor trafficking at excitatory synapses. *Neuron*. 2003; 40(2):361–79. [PubMed: 14556714]
- Buchanan J, Sun YA, Poo MM. Studies of nerve-muscle interactions in *Xenopus* cell culture: fine structure of early functional contacts. *J Neurosci*. 1989; 9(5):1540–54. [PubMed: 2723740]
- Cao G, Harris KM. Developmental Regulation of the Late Phase of Long-Term Potentiation (L-LTP) and Metaplasticity in Hippocampal Area CA1 of the Rat. *J Neurophysiol*. 2012; 107(3):902–12. [PubMed: 22114158]

- Chen X, Winters C, Azzam R, Li X, Galbraith JA, Leapman RD, Reese TS. Organization of the core structure of the postsynaptic density. *Proc Natl Acad Sci U S A*. 2008; 105(11):4453–8. [PubMed: 18326622]
- Choquet D, Triller A. The dynamic synapse. *Neuron*. 2013; 80(3):691–703. [PubMed: 24183020]
- Christie JM, Jahr CE. Multivesicular release at Schaffer collateral-CA1 hippocampal synapses. *J Neurosci*. 2006; 26(1):210–6. [PubMed: 16399689]
- Collingridge GL, Isaac JT, Wang YT. Receptor trafficking and synaptic plasticity. *Nat Rev Neurosci*. 2004; 5(12):952–62. [PubMed: 15550950]
- Dani A, Huang B, Bergan J, Dulac C, Zhuang X. Superresolution imaging of chemical synapses in the brain. *Neuron*. 2010; 68(5):843–56. [PubMed: 21144999]
- Dean C, Scholl FG, Choih J, DeMaria S, Berger J, Isacoff E, Scheiffele P. Neurexin mediates the assembly of presynaptic terminals. *Nat Neurosci*. 2003; 6(7):708–16. [PubMed: 12796785]
- Deane EC, Ilie AE, Sizzdahkhani S, Das GM, Orlowski J, McKinney RA. Enhanced recruitment of endosomal Na⁺/H⁺ exchanger NHE6 into Dendritic spines of hippocampal pyramidal neurons during NMDA receptor-dependent long-term potentiation. *J Neurosci*. 2013; 33(2):595–610. [PubMed: 23303939]
- Derkach VA, Oh MC, Guire ES, Soderling TR. Regulatory mechanisms of AMPA receptors in synaptic plasticity. *Nat Rev Neurosci*. 2007; 8(2):101–13. [PubMed: 17237803]
- deWit J, Sylwestrak E, O'Sullivan ML, Otto S, Tiglio K, Savas JN, Yates JR III, Comoletti D, Taylor P, Ghosh A. LRRTM2 interacts with Neurexin1 and regulates excitatory synapse formation. *Neuron*. 2009; 64(6):799–806. [PubMed: 20064388]
- Dresbach T, Torres V, Wittenmayer N, Altroch WD, Zamorano P, Zuschratter W, Nawrotzki R, Ziv NE, Garner CC, Gundelfinger ED. Assembly of active zone precursor vesicles: obligatory trafficking of presynaptic cytomatrix proteins Bassoon and Piccolo via a trans-Golgi compartment. *J Biol Chem*. 2006; 281(9):6038–47. [PubMed: 16373352]
- Durand GM, Kovalchuk Y, Konnerth A. Long-term potentiation and functional synapse induction in developing hippocampus. *Nature*. 1996; 381(6577):71–5. [PubMed: 8609991]
- Easley-Neal C, Fierro J Jr, Buchanan J, Washbourne P. Late recruitment of synapsin to nascent synapses is regulated by Cdk5 2. *Cell Rep*. 2013; 3(4):1199–212. [PubMed: 23602570]
- Ebbinghaus, H. Über das Gedächtnis: Untersuchungen zur experimentellen Psychologie. Leipzig: Veit & Co; 1885.
- Edwards F. Neurobiology. LTP is a long term problem. *Nature*. 1991; 350(6316):271–2. [PubMed: 1848919]
- Ehlers MD, Heine M, Groc L, Lee MC, Choquet D. Diffusional trapping of GluR1 AMPA receptors by input-specific synaptic activity. *Neuron*. 2007; 54(3):447–60. [PubMed: 17481397]
- Ehrlich I, Klein M, Rumpel S, Malinow R. PSD-95 is required for activity-driven synapse stabilization. *Proc Natl Acad Sci U S A*. 2007; 104(10):4176–81. [PubMed: 17360496]
- Elste AM, Benson DL. Structural basis for developmentally regulated changes in cadherin function at synapses. *J Comp Neurol*. 2006; 495(3):324–35. [PubMed: 16440298]
- Enoki R, Hu YL, Hamilton D, Fine A. Expression of long-term plasticity at individual synapses in hippocampus is graded, bidirectional, and mainly presynaptic: optical quantal analysis. *Neuron*. 2009; 62(2):242–53. [PubMed: 19409269]
- Fannon AM, Colman DR. A model for central synaptic junctional complex formation based on the differential adhesive specificities of the cadherins. *Neuron*. 1996; 17(3):423–34. [PubMed: 8816706]
- Fiala JC. Reconstruct: a free editor for serial section microscopy. *J Microsc*. 2005; 218(Pt 1):52–61. [PubMed: 15817063]
- Fiala JC, Feinberg M, Popov V, Harris KM. Synaptogenesis via dendritic filopodia in developing hippocampal area CA1. *J Neurosci*. 1998; 18(21):8900–11. [PubMed: 9786995]
- Fiala JC, Harris KM. Cylindrical diameters method for calibrating section thickness in serial electron microscopy. *J Microsc*. 2001a; 202(Pt 3):468–72. [PubMed: 11422668]
- Fiala JC, Harris KM. Extending unbiased stereology of brain ultrastructure to three-dimensional volumes. *J Am Med Inform Assoc*. 2001b; 8(1):1–16. [PubMed: 11141509]

- Fiala JC, Kirov SA, Feinberg MD, Petrak LJ, George P, Goddard CA, Harris KM. Timing of neuronal and glial ultrastructure disruption during brain slice preparation and recovery in vitro. *J Comp Neurol*. 2003; 465(1):90–103. [PubMed: 12926018]
- Fifkova E, Anderson CL. Stimulation-induced changes in dimensions of stalks of dendritic spines in the dentate molecular layer. *Exp Neurol*. 1981; 74(2):621–7. [PubMed: 7297640]
- Fifkova E, Van Harrevelde A. Long-lasting morphological changes in dendritic spines of dentate granular cells following stimulation of the entorhinal area. *J Neurocytol*. 1977; 6(2):211–30. [PubMed: 856951]
- Franks KM, Bartol TM Jr, Sejnowski TJ. A Monte Carlo model reveals independent signaling at central glutamatergic synapses. *Biophys J*. 2002; 83(5):2333–48. [PubMed: 12414671]
- Franks KM, Stevens CF, Sejnowski TJ. Independent sources of quantal variability at single glutamatergic synapses. *J Neurosci*. 2003; 23(8):3186–95. [PubMed: 12716926]
- Futai K, Kim MJ, Hashikawa T, Scheiffele P, Sheng M, Hayashi Y. Retrograde modulation of presynaptic release probability through signaling mediated by PSD-95-neuroigin. *Nat Neurosci*. 2007; 10(2):186–95. [PubMed: 17237775]
- Geinisman Y, de Toledo-Morrell L, Morrell F, Heller RE, Rossi M, Parshall RF. Structural synaptic correlate of long-term potentiation: formation of axospinous synapses with multiple, completely partitioned transmission zones. *Hippocampus*. 1993; 3(4):435–45. [PubMed: 8269035]
- Giannone G, Mondin M, Grillo-Bosch D, Tessier B, Saint-Michel E, Czondor K, Sainlos M, Choquet D, Thoumine O. Neurexin-1beta Binding to Neuroigin-1 Triggers the Preferential Recruitment of PSD-95 versus Gephyrin through Tyrosine Phosphorylation of Neuroigin-1. *Cell Rep*. 2013; 3(6):1996–2007. [PubMed: 23770246]
- Graf ER, Zhang X, Jin SX, Linhoff MW, Craig AM. Neurexins induce differentiation of GABA and glutamate postsynaptic specializations via neuroigins. *Cell*. 2004; 119(7):1013–26. [PubMed: 15620359]
- Groc L, Gustafsson B, Hanse E. AMPA signalling in nascent glutamatergic synapses: there and not there! *Trends Neurosci*. 2006; 29(3):132–9. [PubMed: 16443288]
- Hanse E, Taira T, Lauri S, Groc L. Glutamate synapse in developing brain: an integrative perspective beyond the silent state. *Trends Neurosci*. 2009; 32(10):532–7. [PubMed: 19733923]
- Harlow ML, Ress D, Stoschek A, Marshall RM, McMahan UJ. The architecture of active zone material at the frog's neuromuscular junction. *Nature*. 2001; 409(6819):479–84. [PubMed: 11206537]
- Harris KM, Bourne JN, Mendenhall JM, Spacek J. Hippocampal CA1 dendrites of greater caliber have more spines and contain more microtubules as a subcellular supply route [abstract]. *Hippocampal CA1 dendrites of greater caliber have more spines and contain more microtubules as a subcellular supply route*. 2007
- Harris KM, Jensen FE, Tsao B. Three-dimensional structure of dendritic spines and synapses in rat hippocampus (CA1) at postnatal day 15 and adult ages: implications for the maturation of synaptic physiology and long-term potentiation. *J Neurosci*. 1992; 12(7):2685–705. [PubMed: 1613552]
- Harris KM, Perry E, Bourne J, Feinberg M, Ostroff L, Hurlburt J. Uniform serial sectioning for transmission electron microscopy. *J Neurosci*. 2006; 26(47):12101–3. [PubMed: 17122034]
- Harris KM, Stevens JK. Dendritic spines of CA1 pyramidal cells in the rat hippocampus: serial electron microscopy with reference to their biophysical characteristics. *J Neurosci*. 1989; 9(8):2982–97. [PubMed: 2769375]
- Harris KM, Sultan P. Variation in the number, location and size of synaptic vesicles provides an anatomical basis for the nonuniform probability of release at hippocampal CA1 synapses. *Neuropharmacology*. 1995; 34(11):1387–95. [PubMed: 8606788]
- Harvey CD, Yasuda R, Zhong H, Svoboda K. The spread of Ras activity triggered by activation of a single dendritic spine. *Science*. 2008; 321(5885):136–40. [PubMed: 18556515]
- Heine M, Thoumine O, Mondin M, Tessier B, Giannone G, Choquet D. Activity-independent and subunit-specific recruitment of functional AMPA receptors at neurexin/neuroigin contacts. *Proc Natl Acad Sci U S A*. 2008; 105(52):20947–52. [PubMed: 19098102]

- Henkemeyer M, Itkis OS, Ngo M, Hickmott PW, Ethell IM. Multiple EphB receptor tyrosine kinases shape dendritic spines in the hippocampus. *J Cell Biol.* 2003; 163(6):1313–26. [PubMed: 14691139]
- Hering H, Sheng M. Dendritic spines: structure, dynamics and regulation. *Nat Rev Neurosci.* 2001; 2(12):880–8. [PubMed: 11733795]
- Ichchenko K, Hata Y, Nguyen T, Ullrich B, Missler M, Moomaw C, Sudhof TC. Neuroligin 1: a splice site-specific ligand for beta-neurexins. *Cell.* 1995; 81(3):435–43. [PubMed: 7736595]
- Irie M, Hata Y, Takeuchi M, Ichchenko K, Toyoda A, Hirao K, Takai Y, Rosahl TW, Sudhof TC. Binding of neuroligins to PSD-95. *Science.* 1997; 277(5331):1511–5. [PubMed: 9278515]
- Isaac JT, Nicoll RA, Malenka RC. Evidence for silent synapses: implications for the expression of LTP. *Neuron.* 1995; 15(2):427–34. [PubMed: 7646894]
- Jensen FE, Harris KM. Preservation of neuronal ultrastructure in hippocampal slices using rapid microwave-enhanced fixation. *J Neurosci Methods.* 1989; 29(3):217–30. [PubMed: 2507828]
- Kayser MS, McClelland AC, Hughes EG, Dalva MB. Intracellular and trans-synaptic regulation of glutamatergic synaptogenesis by EphB receptors. *J Neurosci.* 2006; 26(47):12152–64. [PubMed: 17122040]
- Kerchner GA, Nicoll RA. Silent synapses and the emergence of a postsynaptic mechanism for LTP. *Nat Rev Neurosci.* 2008; 9(11):813–25. [PubMed: 18854855]
- Kim JH, Udo H, Li HL, Youn TY, Chen M, Kandel ER, Bailey CH. Presynaptic activation of silent synapses and growth of new synapses contribute to intermediate and long-term facilitation in Aplysia. *Neuron.* 2003; 40(1):151–65. [PubMed: 14527440]
- Kinney JP, Spacek J, Bartol TM, Bajaj CL, Harris KM, Sejnowski TJ. Extracellular sheets and tunnels modulate glutamate diffusion in hippocampal neuropil. *J Comp Neurol.* 2013; 521(2):448–64. [PubMed: 22740128]
- Kirov SA, Harris KM. Dendrites are more spiny on mature hippocampal neurons when synapses are inactivated. *Nat Neurosci.* 1999; 2(10):878–83. [PubMed: 10491607]
- Klein R. Bidirectional modulation of synaptic functions by Eph/ephrin signaling. *Nat Neurosci.* 2009; 12(1):15–20. [PubMed: 19029886]
- Kramar EA, Babayan AH, Gavin CF, Cox CD, Jafari M, Gall CM, Rumbaugh G, Lynch G. Synaptic evidence for the efficacy of spaced learning. *Proc Natl Acad Sci U S A.* 2012; 109(13):5121–6. [PubMed: 22411798]
- Lai KO, Ip NY. Synapse development and plasticity: roles of ephrin/Eph receptor signaling. *Curr Opin Neurobiol.* 2009; 19(3):275–83. [PubMed: 19497733]
- Lang C, Barco A, Zablow L, Kandel ER, Siegelbaum SA, Zakharenko SS. Transient expansion of synaptically connected dendritic spines upon induction of hippocampal long-term potentiation. *Proc Natl Acad Sci U S A.* 2004; 101(47):16665–70. [PubMed: 15542587]
- Lavenex P, Lavenex PB, Bennett JL, Amaral DG. Postmortem changes in the neuroanatomical characteristics of the primate brain: hippocampal formation. *J Comp Neurol.* 2009; 512(1):27–51. [PubMed: 18972553]
- Li Z, Sheng M. Some assembly required: the development of neuronal synapses. *Nat Rev Mol Cell Biol.* 2003; 4(11):833–41. [PubMed: 14625534]
- Liao D, Hessler NA, Malinow R. Activation of postsynaptically silent synapses during pairing-induced LTP in CA1 region of hippocampal slice. *Nature.* 1995; 375(6530):400–4. [PubMed: 7760933]
- Lim BK, Matsuda N, Poo MM. Ephrin-B reverse signaling promotes structural and functional synaptic maturation in vivo. *Nat Neurosci.* 2008; 11(2):160–9. [PubMed: 18193042]
- Linhoff MW, Lauren J, Cassidy RM, Dobie FA, Takahashi H, Nygaard HB, Airaksinen MS, Strittmatter SM, Craig AM. An unbiased expression screen for synaptogenic proteins identifies the LRRTM protein family as synaptic organizers. *Neuron.* 2009; 61(5):734–49. [PubMed: 19285470]
- Lisman J, Harris KM. Quantal analysis and synaptic anatomy - integrating two views of hippocampal plasticity. *Trends Neurosci.* 1993; 16:141–7. [PubMed: 7682347]
- Lisman J, Raghavachari S. A unified model of the presynaptic and postsynaptic changes during LTP at CA1 synapses. *Sci STKE.* 2006; (356):re11. [PubMed: 17033044]

- Liu G, Choi S, Tsien RW. Variability of neurotransmitter concentration and nonsaturation of postsynaptic AMPA receptors at synapses in hippocampal cultures and slices. *Neuron*. 1999; 22(2):395–409. [PubMed: 10069344]
- Luscher C, Nicoll RA, Malenka RC, Muller D. Synaptic plasticity and dynamic modulation of the postsynaptic membrane. *Nat Neurosci*. 2000; 3(6):545–50. [PubMed: 10816309]
- Lynch G, Gall CM. Mechanism based approaches for rescuing and enhancing cognition. *Front Neurosci*. 2013; 7:143. [PubMed: 23966908]
- Lynch G, Kramar EA, Babayan AH, Rumbaugh G, Gall CM. Differences between synaptic plasticity thresholds result in new timing rules for maximizing long-term potentiation. *Neuropharmacology*. 2013; 64:27–36. [PubMed: 22820276]
- Maas C, Torres VI, Altroch WD, Leal-Ortiz S, Wagh D, Terry-Lorenzo RT, Fejtova A, Gundelfinger ED, Ziv NE, Garner CC. Formation of Golgi-derived active zone precursor vesicles 12. *J Neurosci*. 2012; 32(32):11095–108. [PubMed: 22875941]
- Macdougall MJ, Fine A. The expression of long-term potentiation: reconciling the preists and the postivists. *Philos Trans R Soc Lond B Biol Sci*. 2014; 369(1633):20130135. [PubMed: 24298138]
- MacGillavry HD, Song Y, Raghavachari S, Blanpied TA. Nanoscale scaffolding domains within the postsynaptic density concentrate synaptic AMPA receptors. *Neuron*. 2013; 78(4):615–22. [PubMed: 23719161]
- Makino H, Malinow R. AMPA receptor incorporation into synapses during LTP: the role of lateral movement and exocytosis. *Neuron*. 2009; 64(3):381–90. [PubMed: 19914186]
- Malinow R, Malenka RC. AMPA receptor trafficking and synaptic plasticity. *Annu Rev Neurosci*. 2002; 25:103–26. [PubMed: 12052905]
- Matsuzaki M, Ellis-Davies GC, Nemoto T, Miyashita Y, Iino M, Kasai H. Dendritic spine geometry is critical for AMPA receptor expression in hippocampal CA1 pyramidal neurons. *Nat Neurosci*. 2001; 4(11):1086–92. [PubMed: 11687814]
- Matsuzaki M, Honkura N, Ellis-Davies GC, Kasai H. Structural basis of long-term potentiation in single dendritic spines. *Nature*. 2004; 429(6993):761–6. [PubMed: 15190253]
- McAllister AK, Stevens CF. Nonsaturation of AMPA and NMDA receptors at hippocampal synapses. *Proc Natl Acad Sci U S A*. 2000; 97(11):6173–8. [PubMed: 10811899]
- McGeachie AB, Cingolani LA, Goda Y. Stabilising influence: integrins in regulation of synaptic plasticity 33. *Neurosci Res*. 2011; 70(1):24–9. [PubMed: 21352859]
- Mendez P, De RM, Poglia L, Klauser P, Muller D. N-cadherin mediates plasticity-induced long-term spine stabilization. *J Cell Biol*. 2010; 189(3):589–600. [PubMed: 20440002]
- Miller DC. Use of perfusion fixation for improved neuropathologic examination. *Arch Pathol Lab Med*. 1998; 122(11):949. [PubMed: 9822120]
- Mishchenko Y, Hu T, Spacek J, Mendenhall J, Harris KM, Chklovskii DB. Ultrastructural analysis of hippocampal neuropil from the connectomics perspective. *Neuron*. 2010; 67(6):1009–20. [PubMed: 20869597]
- Mondin M, Labrousse V, Hosi E, Heine M, Tessier B, Levet F, Pujol C, Blanchet C, Choquet D, Thoumine O. Neurexin-neuroigin adhesions capture surface-diffusing AMPA receptors through PSD-95 scaffolds. *J Neurosci*. 2011; 31(38):13500–15. [PubMed: 21940442]
- Murata Y, Constantine-Paton M. Postsynaptic density scaffold SAP102 regulates cortical synapse development through EphB and PAK signaling pathway. *J Neurosci*. 2013; 33(11):5040–52. [PubMed: 23486974]
- Nagerl UV, Eberhorn N, Cambridge SB, Bonhoeffer T. Bidirectional activity-dependent morphological plasticity in hippocampal neurons. *Neuron*. 2004; 44(5):759–67. [PubMed: 15572108]
- Nair D, Hosi E, Petersen JD, Constals A, Giannone G, Choquet D, Sibarita JB. Super-resolution imaging reveals that AMPA receptors inside synapses are dynamically organized in nanodomains regulated by PSD95. *J Neurosci*. 2013; 33(32):13204–24. [PubMed: 23926273]
- Nolt MJ, Lin Y, Hruska M, Murphy J, Sheffler-Colins SI, Kayser MS, Passer J, Bennett MV, Zukin RS, Dalva MB. EphB controls NMDA receptor function and synaptic targeting in a subunit-specific manner. *J Neurosci*. 2011; 31(14):5353–64. [PubMed: 21471370]

- Nuriya M, Haganir RL. Regulation of AMPA receptor trafficking by N-cadherin. *J Neurochem*. 2006; 97(3):652–61. [PubMed: 16515543]
- Opazo P, Choquet D. A three-step model for the synaptic recruitment of AMPA receptors. *Mol Cell Neurosci*. 2011; 46(1):1–8. [PubMed: 20817097]
- Opazo P, Labrecque S, Tigaret CM, Frouin A, Wiseman PW, De KP, Choquet D. CaMKII triggers the diffusional trapping of surface AMPARs through phosphorylation of stargazin. *Neuron*. 2010; 67(2):239–52. [PubMed: 20670832]
- Ostroff LE, Fiala JC, Allwardt B, Harris KM. Polyribosomes redistribute from dendritic shafts into spines with enlarged synapses during LTP in developing rat hippocampal slices. *Neuron*. 2002; 35(3):535–45. [PubMed: 12165474]
- Owald D, Sigrist SJ. Assembling the presynaptic active zone 34. *Curr Opin Neurobiol*. 2009; 19(3): 311–8. [PubMed: 19395253]
- Petralia RS, Esteban JA, Wang YX, Partridge JG, Zhao HM, Wenthold RJ, Malinow R. Selective acquisition of AMPA receptors over postnatal development suggests a molecular basis for silent synapses. *Nat Neurosci*. 1999; 2(1):31–6. [PubMed: 10195177]
- Raghavachari S, Lisman JE. Properties of quantal transmission at CA1 synapses. *J Neurophysiol*. 2004; 92(4):2456–67. [PubMed: 15115789]
- Ratnayaka A, Marra V, Bush D, Burden JJ, Branco T, Staras K. Recruitment of resting vesicles into recycling pools supports NMDA receptor-dependent synaptic potentiation in cultured hippocampal neurons. *J Physiol*. 2012; 590(Pt 7):1585–97. [PubMed: 22271866]
- Roberts JC, McCrossan MV, Jones HB. The case for perfusion fixation of large tissue samples for ultrastructural pathology. *Ultrastruct Pathol*. 1990; 14(2):177–91. [PubMed: 2345929]
- Ruger, HA.; Bussenius, CE. *Memory: A Contribution to Experimental Psychology*, Hermann Ebbinghaus (1885). New York: Teachers College, Columbia University; 1913.
- Sabo SL, Gomes RA, McAllister AK. Formation of presynaptic terminals at predefined sites along axons. *J Neurosci*. 2006; 26(42):10813–25. [PubMed: 17050720]
- Saglietti L, Dequidt C, Kamieniarz K, Rousset MC, Valnegri P, Thoumine O, Beretta F, Fagni L, Choquet D, Sala C, Sheng M, Passafaro M. Extracellular interactions between GluR2 and N-cadherin in spine regulation. *Neuron*. 2007; 54(3):461–77. [PubMed: 17481398]
- Scheiffele P. Cell-cell signaling during synapse formation in the CNS. *Annu Rev Neurosci*. 2003; 26:485–508. [PubMed: 12626697]
- Scheiffele P, Fan J, Choih J, Fetter R, Serafini T. Neuroligin expressed in nonneuronal cells triggers presynaptic development in contacting axons. *Cell*. 2000; 101(6):657–69. [PubMed: 10892652]
- Schikorski T, Stevens CF. Quantitative ultrastructural analysis of hippocampal excitatory synapses. *J Neurosci*. 1997; 17(15):5858–67. [PubMed: 9221783]
- Shapira M, Zhai RG, Dresbach T, Bresler T, Torres VI, Gundelfinger ED, Ziv NE, Garner CC. Unitary assembly of presynaptic active zones from Piccolo-Bassoon transport vesicles. *Neuron*. 2003; 38(2):237–52. [PubMed: 12718858]
- Sheng M, Kim MJ. Postsynaptic signaling and plasticity mechanisms. *Science*. 2002; 298(5594):776–80. [PubMed: 12399578]
- Shepherd JD, Haganir RL. The cell biology of synaptic plasticity: AMPA receptor trafficking. *Annu Rev Cell Dev Biol*. 2007; 23:613–43. [PubMed: 17506699]
- Shi SH, Hayashi Y, Petralia RS, Zaman SH, Wenthold RJ, Svoboda K, Malinow R. Rapid spine delivery and redistribution of AMPA receptors after synaptic NMDA receptor activation. *Science*. 1999; 284(5421):1811–6. [PubMed: 10364548]
- Shipman SL, Nicoll RA. Dimerization of postsynaptic neuroligin drives synaptic assembly via transsynaptic clustering of neuroligin. *Proc Natl Acad Sci U S A*. 2012; 109(47):19432–7. [PubMed: 23129658]
- Soler-Llavina GJ, Arstikaitis P, Morishita W, Ahmad M, Sudhof TC, Malenka RC. Leucine-rich repeat transmembrane proteins are essential for maintenance of long-term potentiation. *Neuron*. 2013; 79(3):439–46. [PubMed: 23931994]
- Song JY, Ichtchenko K, Sudhof TC, Brose N. Neuroligin 1 is a postsynaptic cell-adhesion molecule of excitatory synapses. *Proc Natl Acad Sci U S A*. 1999; 96(3):1100–5. [PubMed: 9927700]

- Sorra KE, Harris KM. Stability in synapse number and size at 2 hr after long-term potentiation in hippocampal area CA1. *J Neurosci*. 1998; 18(2):658–71. [PubMed: 9425008]
- Sorra KE, Mishra A, Kirov SA, Harris KM. Dense core vesicles resemble active-zone transport vesicles and are diminished following synaptogenesis in mature hippocampal slices. *Neurosci*. 2006; 141(4):2097–106.
- Spacek J, Harris KM. Three-dimensional organization of smooth endoplasmic reticulum in hippocampal CA1 dendrites and dendritic spines of the immature and mature rat. *J Neurosci*. 1997; 17(1):190–203. [PubMed: 8987748]
- Spacek J, Harris KM. Three-dimensional organization of cell adhesion junctions at synapses and dendritic spines in area CA1 of the rat hippocampus. *J Comp Neurol*. 1998; 393(1):58–68. [PubMed: 9520101]
- Stan A, Pielarski KN, Brigadski T, Wittenmayer N, Fedorchenko O, Gohla A, Lessmann V, Dresbach T, Gottmann K. Essential cooperation of N-cadherin and neuroligin-1 in the transsynaptic control of vesicle accumulation. *Proc Natl Acad Sci U S A*. 2010; 107(24):11116–21. [PubMed: 20534458]
- Sudhof TC. Neuroligins and neuexins link synaptic function to cognitive disease. *Nature*. 2008; 455(7215):903–11. [PubMed: 18923512]
- Sytnyk V, Leshchyn'ska I, Delling M, Dityateva G, Dityatev A, Schachner M. Neural cell adhesion molecule promotes accumulation of TGN organelles at sites of neuron-to-neuron contacts. *J Cell Biol*. 2002; 159(4):649–61. [PubMed: 12438412]
- Tang L, Hung CP, Schuman EM. A role for the cadherin family of cell adhesion molecules in hippocampal long-term potentiation. *Neuron*. 1998; 20(6):1165–75. [PubMed: 9655504]
- Traynelis SF, Wollmuth LP, McBain CJ, Menniti FS, Vance KM, Ogden KK, Hansen KB, Yuan H, Myers SJ, Dingledine R. Glutamate receptor ion channels: structure, regulation, and function 27. *Pharmacol Rev*. 2010; 62(3):405–96. [PubMed: 20716669]
- Uchida N, Honjo Y, Johnson KR, Wheelock MJ, Takeichi M. The catenin/cadherin adhesion system is localized in synaptic junctions bordering transmitter release zones. *J Cell Biol*. 1996; 135(3):767–79. [PubMed: 8909549]
- Vaughn JE. Fine structure of synaptogenesis in the vertebrate central nervous system. *Synapse*. 1989; 3(3):255–85. [PubMed: 2655146]
- Waites CL, Craig AM, Garner CC. Mechanisms of vertebrate synaptogenesis. *Annu Rev Neurosci*. 2005; 28:251–74. [PubMed: 16022596]
- Weeks AC, Ivanco TL, LeBoutillier JC, Racine RJ, Petit TL. Sequential changes in the synaptic structural profile following long-term potentiation in the rat dentate gyrus: III. Long-term maintenance phase. *Synapse*. 2001; 40(1):74–84. [PubMed: 11170224]
- Willig KI, Steffens H, Gregor C, Herholt A, Rossner MJ, Hell SW. Nanoscopy of filamentous actin in cortical dendrites of a living mouse. *Biophys J*. 2014; 106(1):L01–L03. [PubMed: 24411266]
- Wittenmayer N, Korber C, Liu H, Kremer T, Varoqueaux F, Chapman ER, Brose N, Kuner T, Dresbach T. Postsynaptic Neuroligin1 regulates presynaptic maturation. *Proc Natl Acad Sci U S A*. 2009; 106(32):13564–9. [PubMed: 19628693]
- Wu YE, Huo L, Maeder CI, Feng W, Shen K. The Balance between Capture and Dissociation of Presynaptic Proteins Controls the Spatial Distribution of Synapses 8. *Neuron*. 2013; 78(6):994–1011. [PubMed: 23727120]
- Yuste R, Bonhoeffer T. Morphological changes in dendritic spines associated with long-term synaptic plasticity. *Annu Rev Neurosci*. 2001; 24:1071–89. [PubMed: 11520928]
- Zhai RG, Vardinon-Friedman H, Cases-Langhoff C, Becker B, Gundelfinger ED, Ziv NE, Garner CC. Assembling the presynaptic active zone: a characterization of an active one precursor vesicle. *Neuron*. 2001; 29(1):131–43. [PubMed: 11182086]
- Zhang P, Lisman JE. Activity-dependent regulation of synaptic strength by PSD-95 in CA1 neurons. *J Neurophysiol*. 2012; 107(4):1058–66. [PubMed: 22114157]
- Ziv NE, Garner CC. Principles of glutamatergic synapse formation: seeing the forest for the trees. *Curr Opin Neurobiol*. 2001; 11(5):536–43. [PubMed: 11595485]
- Ziv NE, Garner CC. Cellular and molecular mechanisms of presynaptic assembly. *Nat Rev Neurosci*. 2004; 5(5):385–99. [PubMed: 15100721]

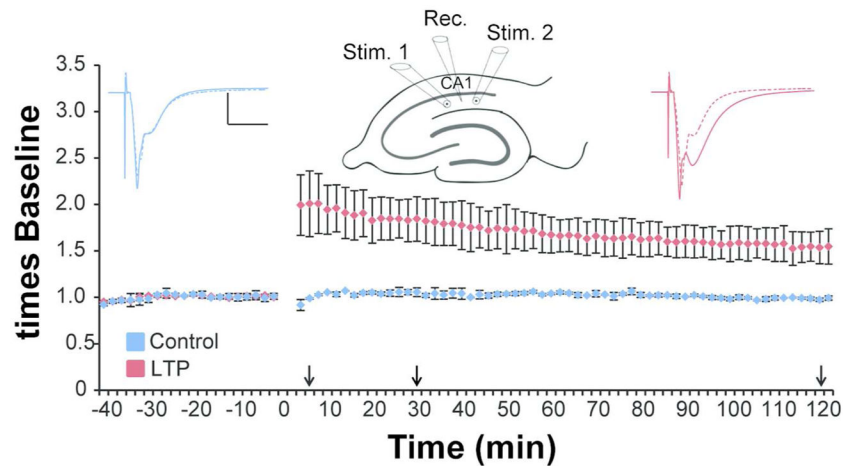


Figure 1.

Site-specific LTP was produced from electrodes positioned in *stratum radiatum* of hippocampal area CA1 and monitored for 5 min ($n=3$ slices from 3 animals), 30 min ($n=3$ slices from 3 animals), or 2 hr ($n=2$ slices from 2 animals) prior to rapid microwave-enhanced fixation. Waveforms are average responses from the control (blue) and TBS (red) stimulation sites, before (dashed lines) and 2 hr after (solid lines) TBS at one site. (Arrows indicate the times when slices were fixed, and scale bars = 5 mV/5 msec.) The graph plots the average responses from the 2 hr experiments. Similar graphs from experiments where the slices were fixed at 5 or 30 min post TBS are published in Bourne and Harris, 2011.

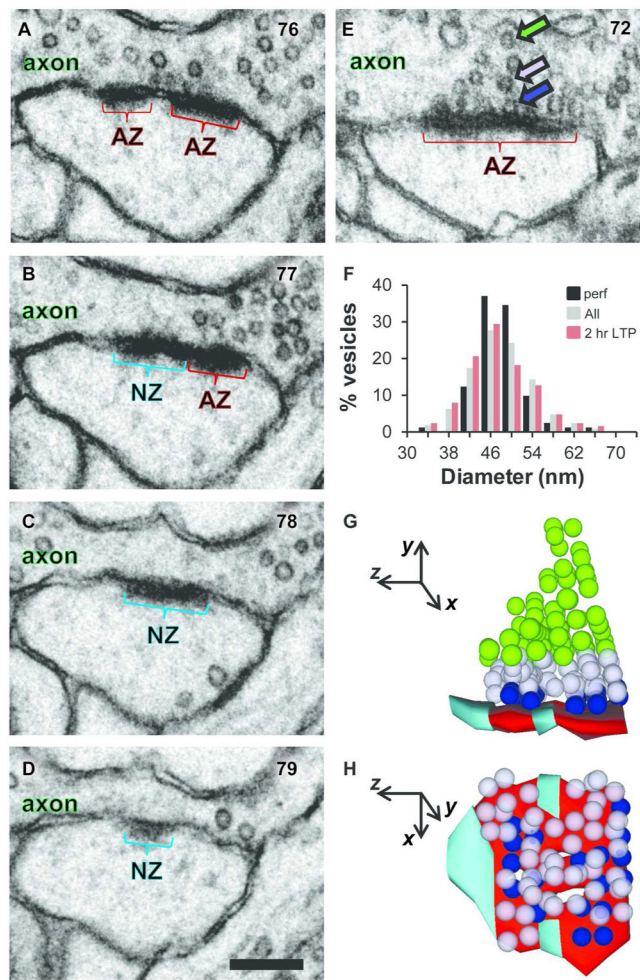


Figure 2.

Delineating nascent zones using 3DEM. (A–D) Four serial sections through a synapse from un-stimulated perfusion-fixed hippocampus show a nascent zone (NZ, aqua) at the edge of an active zone (AZ, red). Section numbers are shown in the upper right corner of each panel. (E) Another section from the same synapse demonstrates presynaptic vesicles that were categorized as docked (in contact with the presynaptic membrane, blue arrow), neighboring nondocked located < 2 vesicle diameters from the presynaptic membrane (light purple arrow), or nondocked and > 2 vesicle diameters from presynaptic membrane (green arrow). (F) Distribution of vesicle diameters is presented as the percentage of vesicles across combined perfusion-fixed and slice conditions ($n = 907$, gray) and compared to the two potential extremes of perfusion-fixed ($n = 81$, black) or 2 hr LTP slices ($n = 126$, red). There were no significant differences in vesicle diameter between any of the series across perfusion-fixed or slice conditions or time (18 total series, one-way ANOVA, $F_{(17,889)} = 1.37$, $p = 0.15$; vesicle numbers from the other conditions were 5 min control, 132 and LTP, 116; 30 min control, 176 and LTP, 187; and 2 hr control, 89). (G) Lateral view of the 3DEM of the synapse in A–E using same color codes. (H) Aerial view illustrates 3 separate NZs. (A–E, G, and H) Images from perfusion-fixed hippocampal area CA1 of a mature rat. Scale

bar in D is 200 nm for A–E, and coordinate system in G–H has the z-direction perpendicular to the serial sections and 100 nm per arrow length.

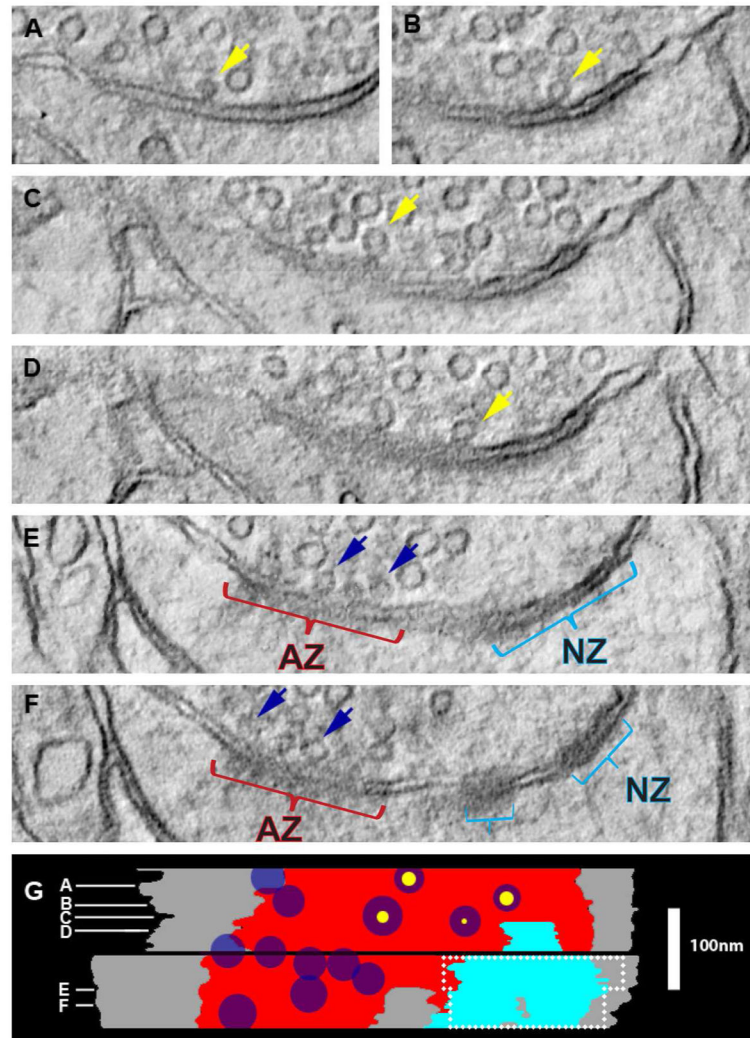


Figure 3.

Identification and measurement of nascent zones in 3DEM using virtual sections computed from transmission EM and tilt tomography. (A–F) Virtual sections from a synapse from perfusion-fixed hippocampus are shown. (A–D) Some docked vesicles had an evident pore (yellow arrows) and (E, F) others were pressed against the presynaptic plasma membrane (blue arrows) when viewed in the 2–3 nm virtual sections. (G) Stacked projection of the axon-spine interface (gray), AZ (red), and NZ (teal) that were first traced through the 2–3 nm virtual sections in RECONSTRUCT™ and then displayed orthogonal to the virtual section planes with white lines illustrating the locations of the virtual sections in (A–F). Maximum diameters of docked vesicles are illustrated as dark blue circles with scaled pores (yellow circles) circumscribed in vesicles that had them. The dashed white line bounds the region in which the same NZ was identified and measured on two of four 50 nm simulated sections for comparison. Approximately 7 nm of tissue appeared to be missing between the two ~120 nm serial sections (black band). Scale in (G) applies to (A–G).

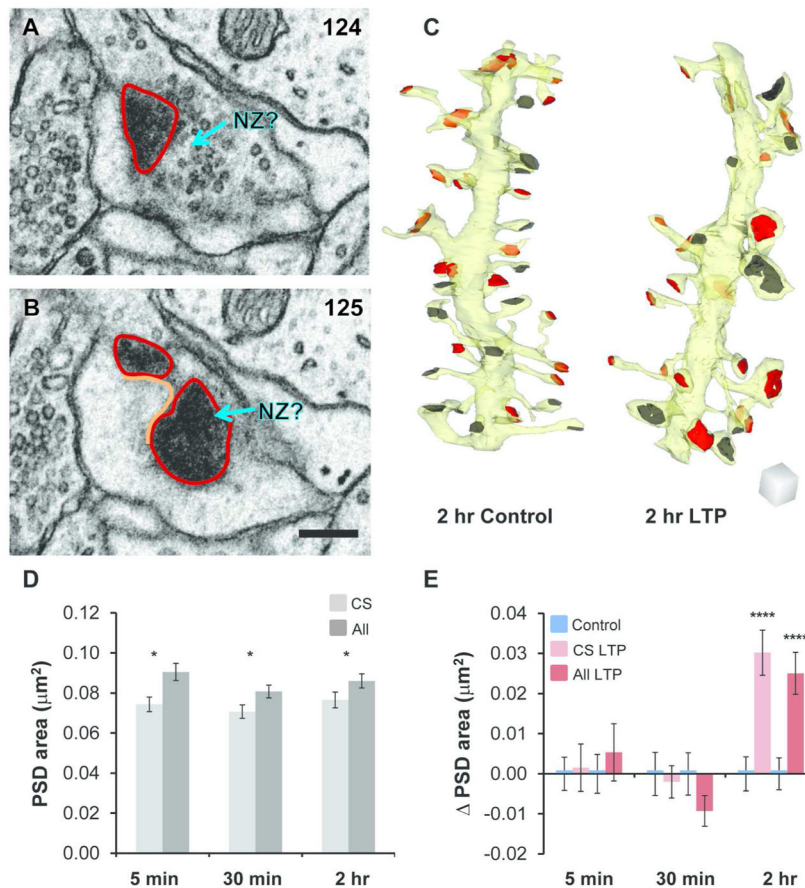


Figure 4.

For accuracy, nascent zone analyses were restricted to cross-sectioned synapses, which revealed the same effects of LTP as in the overall population of synapses. (A–B) An obliquely-sectioned synapse from perfusion-fixed hippocampus with *en face* PSD areas (red) shown in serial sections. These areas were added to a connector line (orange), which was multiplied by section thickness and corresponded to the portion of the synapse that passed between sections. Docked vesicles could have been obscured within the section by the *en face* PSD at a potential NZ (aqua arrow, NZ?). Scale bar is 200 nm. Section numbers are shown in the upper right corner of each panel. (C) 3D reconstructions of sample dendritic segments (yellow) from the 2 hr control and LTP conditions illustrating cross-sectioned PSDs that were included (red) and obliquely sectioned PSDs that were excluded (dark gray) from subsequent analyses. Scale cube is 500 nm per side. (D) When combined across control and LTP slice conditions, the average PSD area from the cross-sectioned subset of synapses (CS, light gray) was significantly less than in the overall population of synapses (All, dark gray; one-way ANOVAs, within time point, 5 min, $F_{(1,851)} = 3.94$, $p = 0.048^*$, CS $n = 335$, All $n = 518$; 30 min, $F_{(1,1061)} = 6.47$, $p = 0.011^*$, CS $n = 437$, All $n = 626$; 2 hr, $F_{(1,989)} = 5.24$, $p = 0.022^*$, CS $n = 399$, All $n = 592$). (E) Changes (Δ) in PSD area for CS synapses (pink) and All synapses (red) relative to time-matched controls were calculated by subtracting the control mean PSD area from each data point by experiment and averaging the results across condition. CS PSD area was unchanged following TBS at 5 min

(hnANOVA, $F_{(1,315)} = 0.49$, $p = 0.49$) and 30 min (hnANOVA, $F_{(1,412)} = 0.36$, $p = 0.55$) but increased significantly at 2 hr during LTP (hnANOVA, $F_{(1,381)} = 24.7$, $p < 0.0001$ ****). Similarly, All PSD area was unchanged following TBS at 5 min (hnANOVA, $F_{(1,498)} = 0.003$, $p = 0.95$) and 30 min (hnANOVA, $F_{(1,601)} = 1.2$, $p = 0.27$) but increased significantly at 2 hr during LTP (hnANOVA, $F_{(1,574)} = 20.5$, $p < 0.0001$ ****). Data were reanalyzed from Bourne and Harris, 2011.

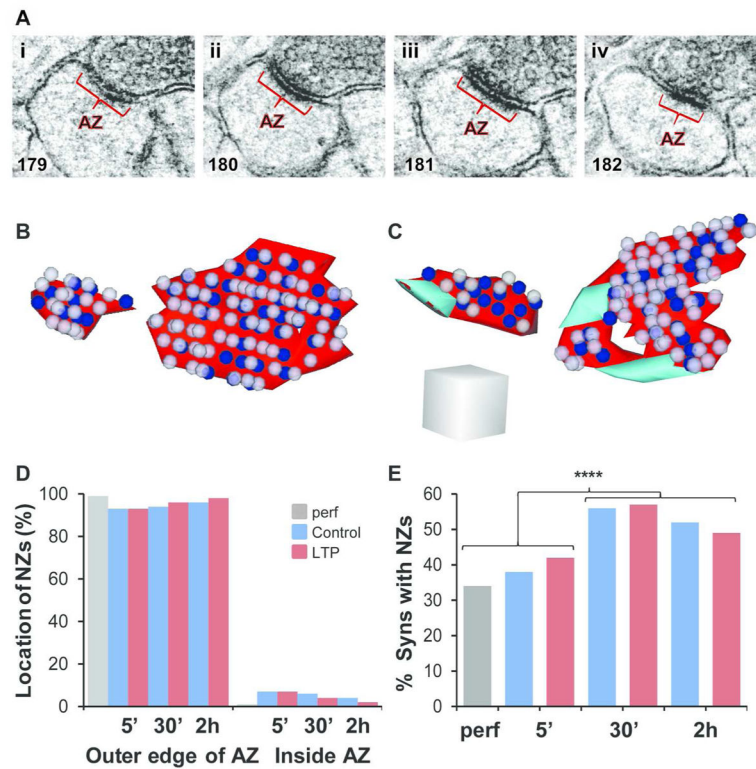


Figure 5.

Location and frequency of nascent zones. (A_{i-iv}) Serial EM images through an AZ (red) without an NZ from the 5 min LTP condition. Section numbers are shown in the lower left corner of each panel. (B) 3DEMs of synapses from various slice conditions as indicated, and with both small and large AZs (red) without NZs, and (C) with NZs (aqua), and docked vesicles (blue) and neighboring non-docked vesicles (light purple). Scale cube is 200 nm per side. (D) NZs were found primarily at the outer edges of AZs and were rarely surrounded by the AZ (inside). (E) The percentage of synapses that had NZs was unaffected by LTP (5 min, $\chi^2 = 0.61$, $p = 0.43$; 30 min, $\chi^2 = 0.04$, $p = 0.84$; 2 hr, $\chi^2 = 0.23$, $p = 0.63$). However, the combined 5 min and perfusion-fixed conditions demonstrated a smaller percentage of synapses with NZs compared to the combined 30 min and 2 hr conditions ($\chi^2 = 28.7$, $p < 0.0001$ ****).

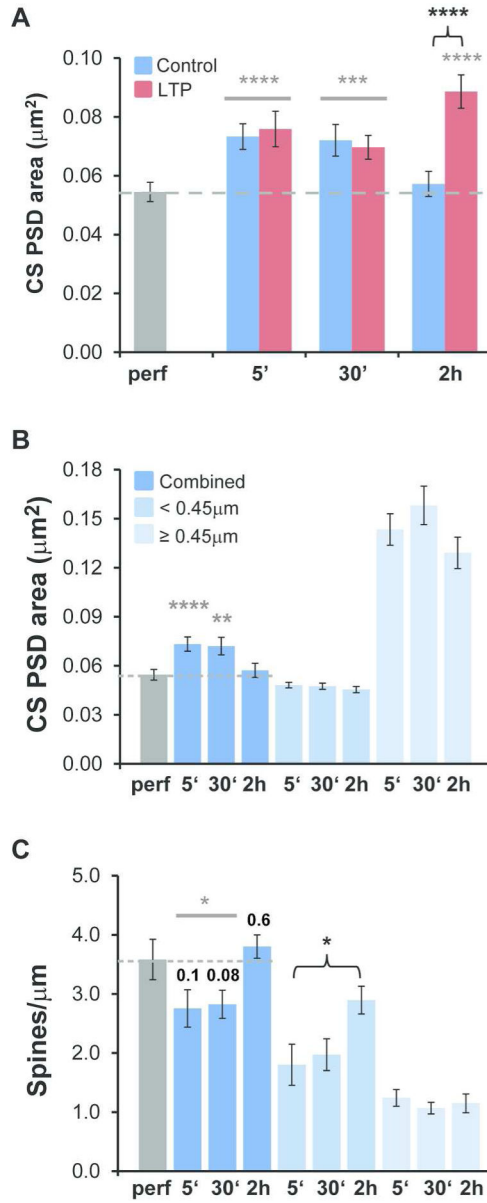


Figure 6.

Restoration of small dendritic spines and average PSD area in acute slices to levels found in perfusion-fixed hippocampus. (A) Relative to perfusion-fixed hippocampus (dashed gray line in each graph), PSD area was increased significantly in slices under both control and LTP conditions at 5 min (hnANOVA, $F_{(1,432)} = 19.2$, $p < 0.0001$, gray****) and 30 min (hnANOVA, $F_{(1,529)} = 7.0$, $p < 0.001$; gray***, but in only two out of three experiments). In the 2 hr LTP condition, PSD area was elevated relative to perfusion-fixed hippocampus (hnANOVA, $F_{(2,498)} = 19.4$, $p < 0.0001$, post-hoc Tukey, $p < 0.0001$, gray****) and the 2 hr control condition (post-hoc Tukey $p < 0.0001$, black bracket****), while the 2 hr control condition was comparable to the perfusion-fixed condition (post-hoc Tukey, $p = 0.97$). (B) Restricting these comparisons to perfusion-fixed versus slice control conditions (data shown in A) revealed greater PSD areas (hnANOVA, $F_{(3,932)} = 10.4$, $p < 0.0001$) at 5 min (post-

hoc Tukey, $p < 0.0001^{****}$) and at 30 min ($p < 0.01^{**}$), but not at 2 hr (post-hoc Tukey, $p = 0.35$). In addition, control PSD areas did not differ significantly among spines with head diameters $< 0.45 \mu\text{m}$ (hnANOVA, $F_{(2,493)} = 0.33$, $p = 0.72$; 5 min $n = 170$, 30 min $n = 183$, and 2 hr $n = 171$) or $\geq 0.45 \mu\text{m}$ (hnANOVA, $F_{(2,260)} = 0.16$, $p = 0.85$, 5 min $n = 122$, 30 min $n = 97$, 2 hr $n = 72$). (C) The control dendrites at 5 and 30 min (combined) had significantly lower spine densities than perfusion-fixed dendrites ($t(28) = 2.1$, $p = 0.044$; p values also shown individually), which were restored to the perfusion-fixed levels by 2 hr in control dendrites ($t(15) = -0.57$, $p = 0.58$). The density of spines with head diameter $< 0.45 \mu\text{m}$ on control dendrites was unchanged between 5 and 30 min ($t(20) = -0.39$, $p = 0.70$) but increased significantly between 5 min and 2 hr ($t(17) = -2.5$, $p = 0.021$, black bracket*). In contrast, the density of spines with head diameter $\geq 0.45 \mu\text{m}$ was unchanged between 5 min and 30 min ($t(20) = 1.0$, $p = 0.31$) or 2 hr ($t(17) = 0.44$, $p = 0.66$) after TBS. The number of dendrites evaluated for spine density in each control condition included: perfusion-fixed, $n = 8$; 5 min, $n = 10$; 30 min, $n = 12$; and 2 hr, $n = 9$.

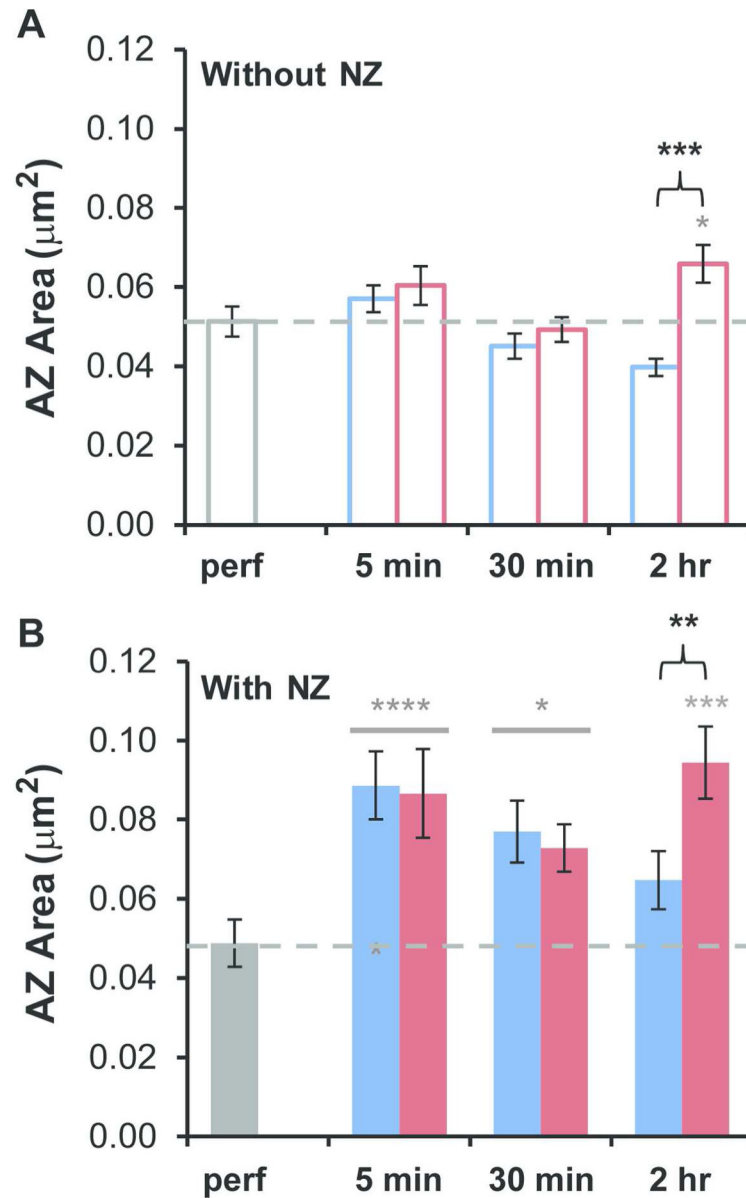


Figure 7.

Influence of the presence of nascent zones on active zone size during constitutive synaptogenesis and LTP. (A) AZ areas at synapses without NZs: Relative to perfusion fixed hippocampus (dashed gray line in each graph), AZ areas were not significantly altered in the combined 5 min (hnANOVA, $F_{(1,257)} = 2.1$, $p = 0.15$) or 30 min (hnANOVA, $F_{(1,238)} = 0.080$, $p = 0.78$) conditions, and increased significantly in the 2 hr LTP condition (hnANOVA, $F_{(2,255)} = 10.7$, $p < 0.0001$; post-hoc Tukey, $p = 0.042$, gray*) but not in the 2 hr control condition (post-hoc Tukey, $p = 0.081$). Relative to time-matched controls, there was no change following TBS at 5 min (hnANOVA, $F_{(1,183)} = 0.021$, $p = 0.89$) or 30 min (hnANOVA, $F_{(1,164)} = 0.024$, $p = 0.88$), although by 2 hr during LTP there was a significant increase (hnANOVA, $F_{(1,181)} = 18.6$, $p < 0.0001$, black bracket***). (B) For synapses with NZs: the AZ areas were significantly increased relative to perfusion-fixed levels for

combined conditions at 5 min (hnANOVA, $F_{(1,147)} = 27.7$, $p < 0.0001$, gray****) and 30 min (hnANOVA, $F_{(1,259)} = 6.1$, $p = 0.014$, gray*, but in only two out of three experiments), and in the 2 hr LTP condition (hnANOVA, $F_{(2,216)} = 10.6$, $p < 0.001$; post-hoc Tukey, $p < 0.001$, gray***), but not in the 2 hr control condition (post-hoc Tukey, $p = 0.32$). Relative to time-matched controls, there were no significant changes following TBS at 5 min (hnANOVA, $F_{(1,111)} = 1.7$, $p = 0.20$) or 30 min (hnANOVA, $F_{(1,223)} = 0.53$, $p = 0.47$); however, the AZs with NZs were larger by 2 hr during LTP (hnANOVA, $F_{(1,180)} = 7.9$, post-hoc Tukey, $p < 0.01$, black bracket**).

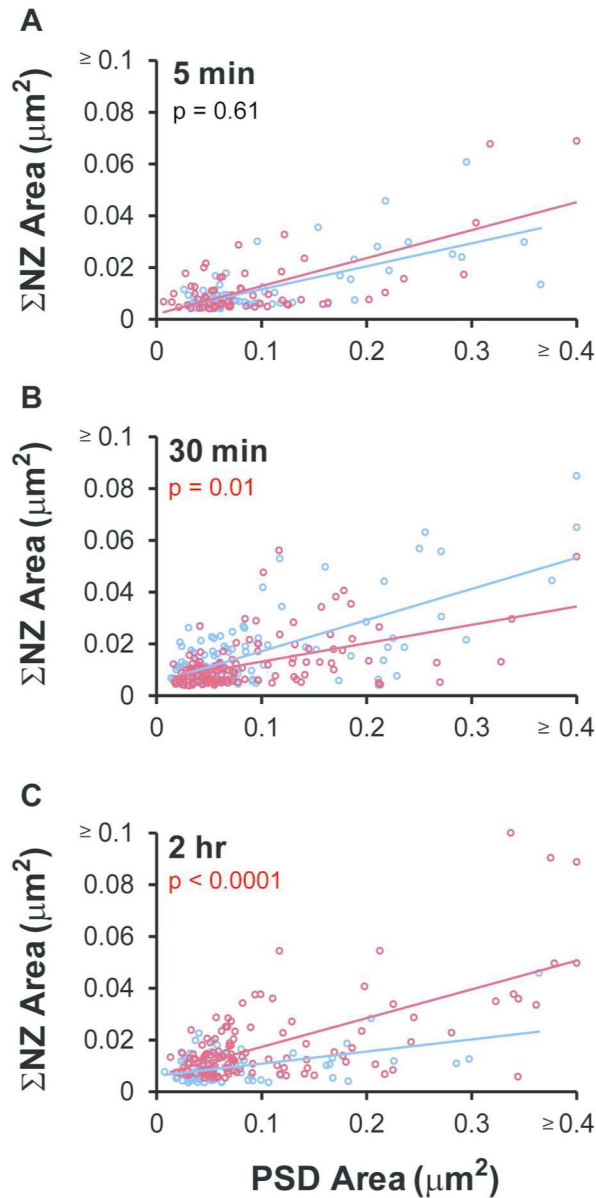


Figure 8.

Direct effects of LTP on nascent zones. (A) The summed NZ area per synapse was correlated with PSD area but did not change following TBS at 5 min (control, $r = 0.69$, $p < 0.0001$; LTP, $r = 0.73$, $p < 0.0001$; ANCOVA, $F_{(1,125)} = 0.28$, $p = 0.60$) or (B) at 30 min (control, $r = 0.72$, $p < 0.0001$; LTP, $r = 0.52$, $p < 0.0001$; ANCOVA, $F_{(1,241)} = 7.4$, $p < 0.01$). (C) Summed NZ area remained well-correlated with PSD area in the 2 hr condition, and increased significantly during LTP (control, $r = 0.49$, $p < 0.0001$; LTP, $r = 0.65$, $p < 0.0001$; ANCOVA, $F_{(1,195)} = 11.4$, $p < 0.001$). For PSD areas $\geq 0.4 \mu\text{m}^2$ and NZ areas $\geq 0.1 \mu\text{m}^2$ the following points are plotted: 5 min LTP ($0.61 \mu\text{m}^2$, $0.069 \mu\text{m}^2$), 30 min control ($0.43 \mu\text{m}^2$, $0.065 \mu\text{m}^2$; $0.61 \mu\text{m}^2$, $0.085 \mu\text{m}^2$), 30 min LTP ($0.54 \mu\text{m}^2$, $0.054 \mu\text{m}^2$), and 2 hr LTP ($0.34 \mu\text{m}^2$, $0.12 \mu\text{m}^2$; $0.66 \mu\text{m}^2$, $0.089 \mu\text{m}^2$; $0.62 \mu\text{m}^2$, $0.050 \mu\text{m}^2$).

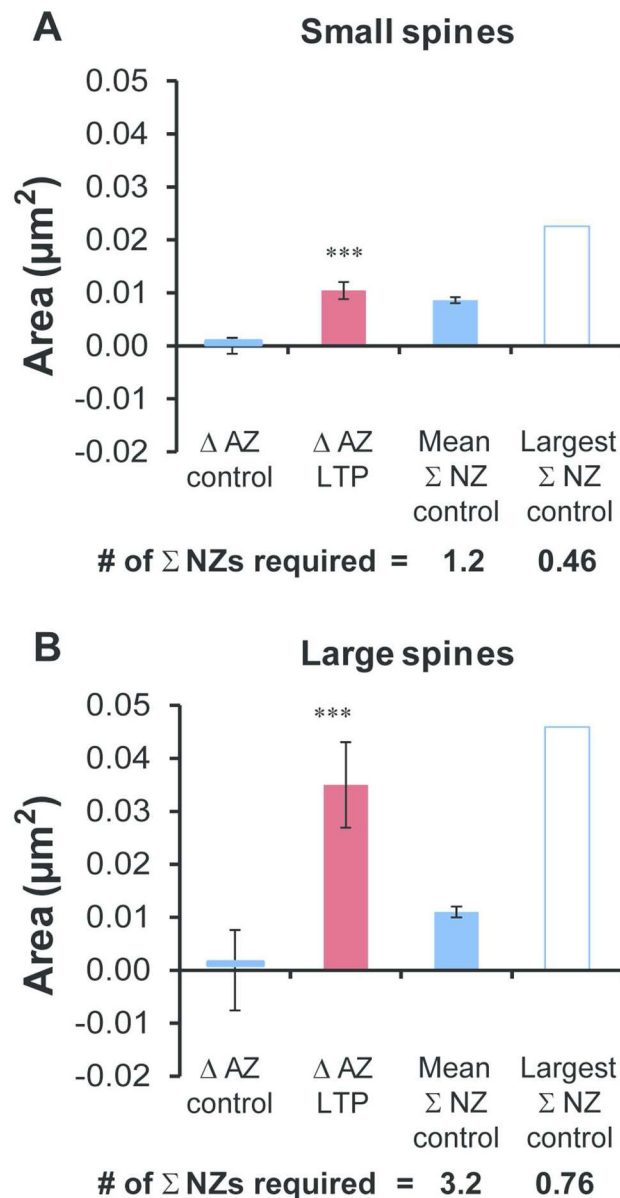


Figure 9. Determining whether nascent zones were large enough to account for active zone growth at 2 hr during LTP. (A) AZ area increased significantly during LTP on small spines (head diameter $< 0.36 \mu\text{m}$, hnANOVA, $F_{(1,167)} = 12.5$, $p < 0.001^{***}$) and (B) large spines (head diameter $> 0.36 \mu\text{m}$, hnANOVA, for LTP, $F_{(1,194)} = 13.5$, $p < 0.001^{***}$). Changes () were calculated by subtracting the control mean AZ area from each data point by experiment and averaging the results across condition to compare changes in AZ area to summed (Σ) NZ areas. The mean and largest summed NZ areas that were found on small or large spines in the 2 hr control condition are plotted, as are the number of each required to be converted to achieve the mean AZ enlargement at 2 hr during LTP.

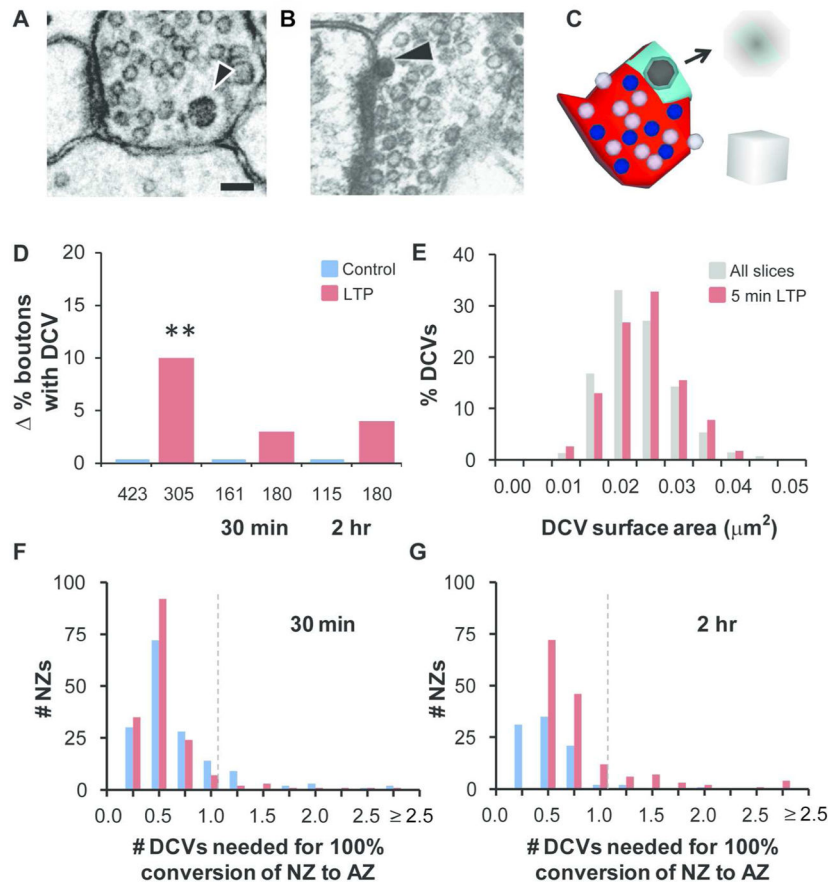


Figure 10.

Presynaptic dense core vesicles (DCVs) and nascent zone conversions during LTP. (A) DCVs were identified (arrowhead) in the presynaptic boutons of cross-sectioned synapses from slice experiments and combined for frequency analyses with findings from synapses sectioned in all orientations. (B) DCV (arrowhead) fusing with presynaptic membrane (image from a recovered mature hippocampal slice, previously published in Sorra et al., 2006). Scale bar in A is 100 nm for A–B. (C) Proposed DCV involvement in nascent to active zone conversion. 3D reconstruction with AZ (red), NZ (aqua), DCV (black), docked vesicles (blue), and neighboring nondocked vesicles (light purple). Arrow annotates DCV insertion and overlap at a nascent zone. Scale cube is 100 nm per side. (D) Comparisons to time-matched controls show an increase in the percentage of boutons with DCVs at 5 min after TBS ($\chi^2 = 9.87$, $p < 0.01^{**}$; control 20%, $n = 423$ boutons; LTP 30%, $n = 305$ boutons), but not at 30 min ($\chi^2 = 0.25$, $p = 0.62$; control 43%, $n = 161$; LTP 46%, $n = 180$) or 2 hr during LTP ($\chi^2 = 0.51$, $p = 0.47$; control 30%, $n = 115$; LTP 34%, $n = 180$). Changes () were calculated by subtracting control percentages from LTP percentages at each time point. (E) DCV surface areas are plotted as percent of all the measured DCVs from slices (gray) and from just the 5 min LTP condition (red). The DCV diameters used to calculate DCV surface areas did not differ across slice conditions (main effects ANOVA, time point: $F_{(2,822)} = 0.44$, $p = 0.64$; condition: $F_{(1,822)} = 2.36$, $p = 0.12$, see also Table 2). (F, G) Individual NZ areas were divided by the overall mean DCV surface area in slices ($0.021 \pm$

0.0002 μm^2), and the resulting distribution of the number of DCVs that would be needed for their full conversion to AZ area is shown at (F) 30 min (control mean = 0.54 ± 0.03 , LTP mean = 0.46 ± 0.02) and (G) 2 hr (control mean = 0.40 ± 0.03 , LTP mean = 0.69 ± 0.05). Dotted line indicates 1 DCV necessary for full conversion.

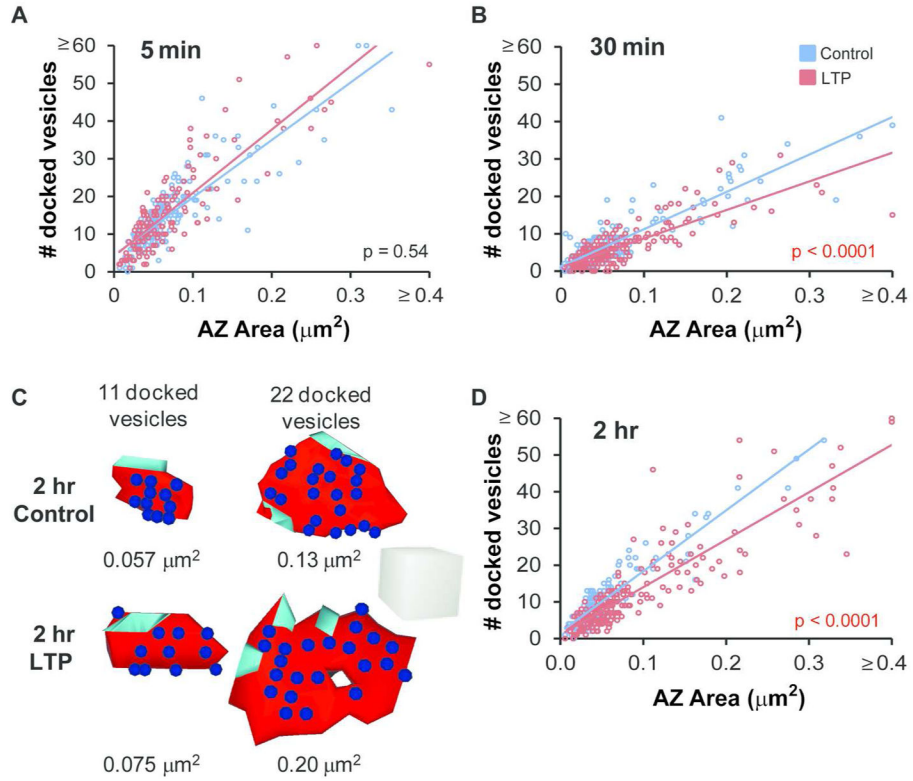


Figure 11.

The density of docked vesicles decreased as active zones were enlarged during LTP. (A) The density of docked vesicles per AZ area was correlated with PSD area and unchanged at 5 min after TBS relative to control stimulation (control, $r = 0.86$, $p < 0.0001$; LTP, $r = 0.83$, $p < 0.0001$; ANCOVA, $F_{(1,327)} = 0.37$, $p = 0.54$). (B) By 30 min after TBS, the density of docked vesicles per AZ area remained well correlated with AZ area; however, the density decreased relative to control stimulation (control, $r = 0.87$, $p < 0.0001$; LTP, $r = 0.79$, $p < 0.0001$; ANCOVA, $F_{(1,430)} = 21.7$, $p < 0.0001$). (C) 3D examples of small and large synapses illustrate representative docked vesicle distributions at AZs in the 2 hr control and LTP conditions. Scale cube, 200 nm per side. (D) Docked vesicle density remained well correlated with AZ area but decreased by 2 hr during LTP (control, $r = 0.94$, $p < 0.0001$; LTP, $r = 0.89$, $p < 0.0001$; ANCOVA, $F_{(1,392)} = 34.6$, $p < 0.0001$). Several points were included in the AZ area $> 0.4 \mu\text{m}^2$ and docked vesicle number > 60 categories, including: 5 min control ($0.32 \mu\text{m}^2$, 75; $0.31 \mu\text{m}^2$, 65) and LTP ($0.54 \mu\text{m}^2$, 55; $0.26 \mu\text{m}^2$, 62), 30 min control ($0.52 \mu\text{m}^2$, 39) and LTP ($0.49 \mu\text{m}^2$, 15), and 2 hr LTP ($0.57 \mu\text{m}^2$, 59; $0.57 \mu\text{m}^2$, 69).

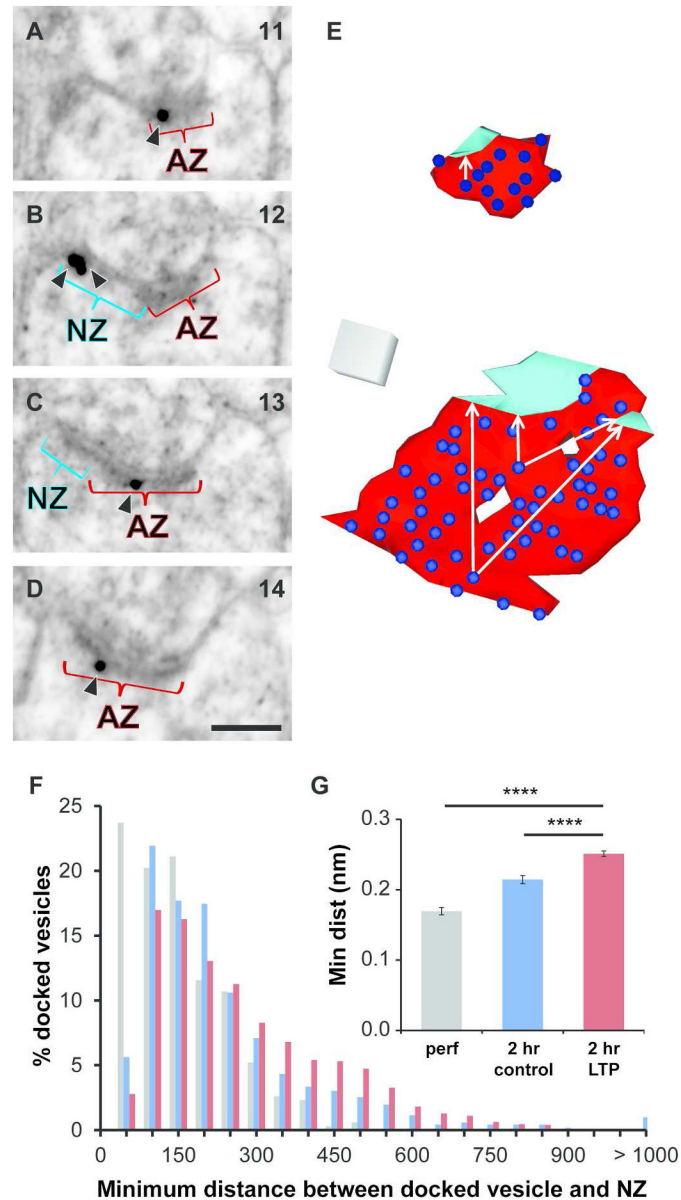


Figure 12.

Proximity of nascent zones to glutamate release sites. (A–D) Four serial sections from an unstimulated hippocampal slice illustrates gold-labeled GluA1 (arrowheads), NZ (aqua), and AZ (red). GluA1 labeling was found in the NZ (B) and in the AZ (A, C, D). Scale bar is 500 nm. Section numbers from the series are labeled in the upper right corner. (E) 3D reconstruction of an average-sized synapse with one NZ (top) and a large synapse with two NZs (bottom), both from the 2 hr LTP condition. AZ (red), NZs (aqua), and docked vesicles (blue) with white arrows illustrating example distances measured from docked vesicles to an edge of the NZs. (F) Distribution of minimum distances between each docked vesicle and NZ(s) on the same synapse in the perfusion-fixed (gray) and 2 hr control (blue) and LTP (red) conditions. (G) Mean minimum distance between docked vesicles and NZ(s) increased in the 2 hr LTP condition relative to perfusion-fixed hippocampus (hnANOVA, $F_{(1,3811)} =$

60.2, $p < 0.0001$; post-hoc Tukey $p < 0.0001^{****}$) and 2 hr control (post-hoc Tukey $p < 0.0001^{****}$).

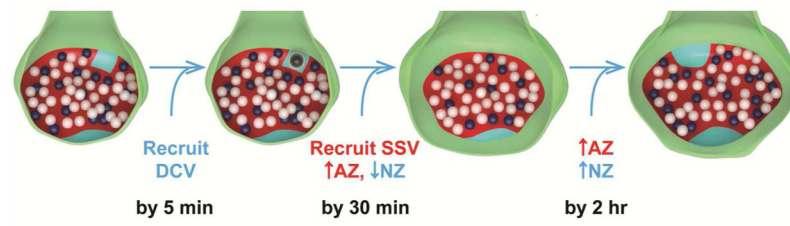


Figure 13.

Model incorporating nascent zone conversion and growth during the synaptic plasticity associated with LTP. Colors represent: axonal bouton (green), AZ (red), NZs (aqua), DCV (dark gray), docked vesicles (dark blue), and nondocked small synaptic vesicles located within 94 nm of the presynaptic membrane (white).

Table 1

Sample of cross-sectioned synapses.

Condition	Description	PSD area (μm^2)	AZ area (μm^2)	NZ area (μm^2)	# NZ/PSD
Perfusion-fixed	N	124	124	48	43
	mean \pm SD	0.054 \pm 0.037	0.050 \pm 0.035	0.011 \pm 0.009	1.1 \pm 0.4
	range	0.013 – 0.169	0.009 – 0.169	0.005 – 0.051	3
5 min control	N	189	189	95	71
	mean \pm SD	0.073 \pm 0.060	0.069 \pm 0.055	0.009 \pm 0.005	1.3 \pm 0.8
	range	0.007 – 0.366	0.007 – 0.353	0.004 – 0.032	4
5 min LTP	N	146	145	72	61
	mean \pm SD	0.076 \pm 0.073	0.071 \pm 0.067	0.010 \pm 0.009	1.2 \pm 0.6
	range	0.007 – 0.609	0.007 – 0.540	0.004 – 0.052	4
30 min control	N	201	201	161	113
	mean \pm SD	0.072 \pm 0.076	0.063 \pm 0.067	0.011 \pm 0.009	1.4 \pm 0.8
	range	0.006 – 0.610	0.002 – 0.525	0.004 – 0.058	5
30 min LTP	N	236	236	168	135
	mean \pm SD	0.070 \pm 0.062	0.063 \pm 0.058	0.010 \pm 0.008	1.2 \pm 0.6*
	range	0.011 – 0.544	0.004 – 0.490	0.004 – 0.056	4
2 hr control	N	153	152	92	79
	mean \pm SD	0.057 \pm 0.053	0.053 \pm 0.050	0.008 \pm 0.005	1.2 \pm 0.4
	range	0.006 – 0.364	0.006 – 0.318	0.004 – 0.039	3
2 hr LTP	N	246	245	153	121
	mean \pm SD	0.089 \pm 0.089****	0.080 \pm 0.081****	0.015 \pm 0.012****	1.3 \pm 0.6
	range	0.006 – 0.661	0.006 – 0.572	0.005 – 0.082	5

Includes: number of synapses (N), mean \pm standard deviation (SD), and ranges for PSD, AZ, and NZ areas, and the maximum number of NZs per synapse for synapses that had NZs (#NZ/PSD) for perfusion-fixed tissue and control and LTP slices at increasing experimental time points. Statistical comparisons of LTP versus time-locked controls for AZ areas (hnANOVAs, 5 min, $F(1,314) = 0.63$, $p = 0.43$; 30 min, $F(1,412) = 1.2$, $p = 0.27$; 2 hr, $F(1,379) = 22.1$, $p < 0.0001$ ****), Statistical comparisons of LTP versus time-locked controls for individual NZ areas (hnANOVAs, 5 min, $F(1,147) = 0.54$, $p = 0.46$; 30 min, $F(1,304) = 2.0$, $p = 0.16$; 2 hr, $F(1,227) = 42.1$, $p < 0.0001$ ****) and for the number of NZs per PSD (hnANOVAs, 5 min, $F(1,112) = 3.3$, $p = 0.071$; 30 min, $F(1,223) = 4.6$, $p = 0.032$ *, and 2 hr, $F(1,182) = 3.0$, $p = 0.084$).

Table 2

Sample of dense core vesicles and docked vesicles.

Condition	Description	# DCV/Bouton	# docked vesicles
Perfusion-fixed	N	37	124
	mean \pm SD	2.1 \pm 1.4	6.2 \pm 4.8
	maximum	6	24
5 min control	N	51	189
	mean \pm SD	1.9 \pm 1.2	15 \pm 10
	maximum	7	75
5 min LTP	N	39	145
	mean \pm SD	1.8 \pm 1.1	16 \pm 12
	maximum	5	62
30 min control	N	69	201
	mean \pm SD	1.9 \pm 1.4	7.4 \pm 7.2
	maximum	8	41
30 min LTP	N	81	236
	mean \pm SD	1.7 \pm 1.2	5.8 \pm 5.2*
	maximum	7	31
2 hr control	N	35	152
	mean \pm SD	1.66 \pm 0.97	10.5 \pm 8.8
	maximum	4	54
2 hr LTP	N	62	245
	mean \pm SD	1.4 \pm 1.0	11.3 \pm 10.8
	maximum	8	69

N = the number of boutons analyzed for percentage of boutons with DCVs and the number of docked vesicles per bouton. The mean \pm standard deviation (SD) and ranges are provided for the number of DCVs per bouton (including only boutons that had at least 1 DCV) for the number of docked vesicles per synapse. Statistical comparisons of LTP versus time-locked controls: for number of DCVs per bouton (main effects ANOVAs: 5 min, $F(1,85) = 0.15$, $p = 0.70$; 30 min, $F(1,146) = 0.63$, $p = 0.43$; 2 hr, $F(1,94) = 1.2$, $p = 0.28$) and for docked vesicles per synapse (lnANOVAs, 5 min, $F(1,313) = 0.33$, $p = 0.57$; 30 min, $F(1,401) = 4.6$, $p = 0.032^*$; 2 hr, $F(1,377) = 0.028$, $p = 0.87$).